



Applications of spatial light modulators in Raman spectroscopy

Journal:	<i>Applied Spectroscopy</i>
Manuscript ID	ASP-18-0370.R1
Manuscript Type:	Focal Point Review
Date Submitted by the Author:	n/a
Complete List of Authors:	Sinjab, Faris; University of Nottingham, School of Physics and Astronomy; University of Tokyo, Department of Physics Liao, Zhiyu; University of Nottingham, School of Physics and Astronomy Notingher, Ioan ; University of Nottingham, School of Physics and Astronomy
Manuscript Keywords:	Raman spectroscopy, Spatial light modulators, Instrumentation, Novel techniques
Abstract:	Advances in consumer display screen technologies have historically been adapted by researchers across the fields of optics as they can be used as electronically controlled spatial light modulators (SLMs) for a variety of uses. The performance characteristics of such SLM devices based on liquid crystal (LC) and digital-micro-mirror device (DMD) technologies in particular has developed to the point where they are compatible with increasingly sensitive instrumental applications, for example Raman spectroscopy. SLMs provide additional flexibility, from modulation of the laser excitation (including multiple laser foci patterns), manipulation of microscopic samples (optical trapping) or selection of sampling volume (adaptive optics or spatially offset Raman spectroscopy), to modulation in the spectral domain for high-resolution spectral filtering or multiplexed/compressive fast detection. Here, we introduce the benefits of different SLM devices as a part of Raman instrumentation, and provide a variety of recent example applications which have benefited from their incorporation into a Raman system.

SCHOLARONE™
Manuscripts

Applications of Spatial Light Modulators in Raman Spectroscopy

Faris Sinjab^{1,2}, Zhiyu Liao¹, Ioan Notingher^{1*}

¹ School of Physics, University of Nottingham, Nottingham, NG7 2RD, UK

² Current address: Department of Physics, University of Tokyo, Tokyo, 113-0033, Japan

*Email: ioan.notingher@nottingham.ac.uk

Advances in consumer display screen technologies have historically been adapted by researchers across the fields of optics as they can be used as electronically controlled spatial light modulators (SLMs) for a variety of uses. The performance characteristics of such SLM devices based on liquid crystal (LC) and digital-micro-mirror device (DMD) technologies in particular has developed to the point where they are compatible with increasingly sensitive instrumental applications, for example Raman spectroscopy. SLMs provide additional flexibility, from modulation of the laser excitation (including multiple laser foci patterns), manipulation of microscopic samples (optical trapping) or selection of sampling volume (adaptive optics or spatially offset Raman spectroscopy), to modulation in the spectral domain for high-resolution spectral filtering or multiplexed/compressive fast detection. Here, we introduce the benefits of different SLM devices as a part of Raman instrumentation, and provide a variety of recent example applications which have benefited from their incorporation into a Raman system.

Keywords: Raman spectroscopy, spatial light modulators, Instrumentation, Novel methods

Introduction

Raman spectroscopy has continually benefited from a variety of scientific and technological advances. For spontaneous Raman spectroscopy, back-thinned CCD

1
2
3 detectors allowed electronic readout of high-quality spectra at reasonable speeds [1], high-
4 power narrow-linewidth near-infrared lasers provide almost ideal excitation sources for
5 biological samples [2] and high-fidelity optical filters now boast excellent rejection of
6 excitation light with sharp edges close to the excitation frequency[3]. Coupling of these
7 advanced optoelectronic devices to optical or completely different instruments such as
8 scanning probe microscopes has enabled probing the molecular structure of materials with
9 micro- or nanometer scale spatial resolution[4, 5]. All these advances have transformed
10 Raman spectroscopy from an expensive specialist technique to common bench-top
11 instrument used across the physical and life sciences[6, 7, 8]. Of course, advances in
12 technology continue, with new and seemingly far-removed areas of optics finding uses in
13 Raman spectroscopy instrumentation.
14
15

16
17 In this focal point review, we will describe the use of a class of devices termed spatial light
18 modulator (SLM), which are increasingly used in various ways for both spontaneous and
19 nonlinear Raman spectroscopic measurement. Most SLM device technologies were
20 originally developed for use as digital display screen technology, where large arrays of
21 individual electronically addressable pixels must rapidly modulate light by some physical
22 means to produce an image. Perhaps the most familiar example of such a technology is the
23 liquid-crystal display (LCD), where electronic control of the liquid crystal orientation
24 allows control of optical polarization, and, in combination with a polarizer, amplitude
25 modulation of a backlight.
26
27

28 Historically, the prevalence of low-cost consumer LCDs led to their modification and use
29 in optical instruments [9]. Here, instead of the amplitude modulation of an incoherent
30 broad-band backlight used for display purposes, laser light was directed onto the liquid
31 crystal. As laser light is coherent, an ideal spatial cross section of a laser beam will be
32 constant in phase. An LCD screen can modulate the phase by some amount at each pixel
33 at which some proportion of the laser passes through, as illustrated in Figure 1 (a-c). This
34 is the basis for a variety of subsequent techniques, which utilize the spatially-modulated
35 phase of the laser in some way as shown schematically in Figure 2.
36
37

38
39 Figure 1. Basic concept of phase (a-c) and amplitude (d-f) spatial light modulation. (a) A
40 simulated 8-bit SLM pattern, the bottom row of which is shown in (b), demonstrating the
41 correspondence of image bit value with some phase value. The physical effect of this on a
42 constant phase laser wavefront is shown in (c). A binary modulation pattern is shown in
43 (d), with the data values, which correspond to the direction of a single micro-mirror,
44 shown in (e). For an incident wavefront, this will direct part of the light $+\theta$, and the rest
45 in the $-\theta$ direction.
46
47
48

49 One example is for using the spatial-phase modulation to imprint a holographic pattern
50 onto a continuous-wave (CW) laser wavefront. Placing the LCD in the back-focal plane of
51 a lens will result in a Fourier-transform of the spatially varying phase pattern imprinted on
52 the laser at the front focal point. With appropriate choice of phase-hologram, the incident
53 laser can be modulated to focus to multiple spatially separated points, allowing computer-
54 control of multiple laser foci, as used for optical trapping[9] and multi-foci laser scanning
55
56
57
58
59
60

1
2
3 microscopy[10, 11]. LC-SLMs have also commonly been used for shaping ultrafast laser
4 pulses[12] and aberration correction of optical systems[13, 14].
5

6
7 More recent projection display technologies involve completely different approaches to
8 light modulation based on micro-electro-mechanical systems (MEMS). The most
9 successful MEMS display technology is the digital micro-mirror device (DMD) developed
10 by Texas Instruments. These devices utilize arrays of microscopic mirrors (pixel units)
11 whose reflection direction can be individually controlled electronically. Modern digital
12 projectors utilize DMD technology, where video frames are generated by rapidly switching
13 DMD patterns which provides spatial modulation of light amplitude to form the individual
14 colour channel image (different colours of which are generated sequentially).
15

16
17 Amplitude modulation with DMDs has been used for a variety of applications in optics,
18 from single-pixel compressive sensing cameras [15, 16] and spatially-encoded
19 fluorescence spectroscopic imaging [17], to their use as computer-controlled reflective
20 apertures[18]. Many of these optical applications have focused on bright-field and
21 fluorescence microscopy, where DMDs can modify the light fields in some desirable way
22 as shown in Figure 1 (d-f), to improve aspects of measurement such as speed or spatial
23 resolution.
24

25
26 The use of SLMs in other areas of optical sensing preceded their use in Raman
27 spectroscopy, which typically requires high-fidelity optical components to allow efficient
28 excitation and detection, as Raman scattering is a notoriously inefficient process compared
29 to laser-induced fluorescence emission or elastic scattering (typically 5-7 orders of
30 magnitude lower). However, with the improvement of the optical throughput of SLMs,
31 laser excitation and Raman detection losses have approached an acceptable operational
32 range for their usage into Raman spectroscopy instruments.
33

34
35 This review will first describe commonly used SLM devices (primarily LC-SLMs and
36 DMDs), their basic function, and some important parameters to consider for their use.
37 Following this, we will review examples of SLMs used in Raman spectroscopy,
38 highlighting examples where phase-only, amplitude only or phase and amplitude
39 modulation in combination SLMs are utilized. We finish by discussing the outlook for
40 SLMs applied to Raman spectroscopy, and potential new areas for exploration.
41
42
43
44

45 Figure 2. Illustration of types of spatial light modulation relevant to Raman spectroscopy.
46 Common examples include excitation beam cross-sections, spectrally dispersed
47 excitation pulse or spectrally modulated light detection. Patterns can include those
48 corresponding to holographic, spatial, or spectral modulation. Results of these
49 modulations involve multi-point illumination or spatial/spectral modulation. Other types
50 of modulation may be possible. Importance of position of where LC-SLM placed in
51 optical system.
52

53 54 SLM devices 55 56 57 58 59

Phase modulation with liquid-crystal spatial light modulators

The LC-SLM is perhaps the most widely utilized SLM device, as liquid crystal technology was one of the earliest digital display screen technologies, the success of which has since led to them becoming relatively low-cost and widespread. Generally, LC-SLMs are phase modulation devices, where controlled phase delay is achieved pixel-by-pixel by electronic control of liquid crystal orientation axis. Nematic liquid crystals are almost exclusively used for 1D or 2D LC-SLMs.

The degree to which a liquid crystal is rotated determines the relative phase-shift of the light at each pixel (note: this implies the impinging light is polarized at a particular angle for efficient modulation). LC-SLMs are usually utilized in reflection mode as the LC control substrate is typically silicon (sometimes specified as liquid crystal on silicon (LCOS)-SLMs) with a high-reflectance layer. Transmission-mode LC-SLMs exist, though are typically lower resolution and have lower optical throughput compared with their reflective counterparts.

LC-SLMs can often modulate broad spectral regions of light, from 400-1600nm, though the total phase shift will vary depending on the exact wavelength. Anti-reflective coatings can be utilized to improve throughput for a particular spectral range. The throughput also depends on other factors than reflection, such as the fill factor (percentage of total display area which can be utilized, related to dead-space between active pixel regions), and the light utilization efficiency (fraction of total incident light which is controllably modulated). Modulation speed is typically in the range of commercial display screen refresh rates (60-120Hz), though with GPU acceleration this can be further increased[19, 20]. New devices developed by Meadowlark are also capable of faster refresh rates approaching 1 kHz.

The major manufacturers of LC-SLMs for scientific applications are Hamamatsu, Holoeye and Meadowlark (formerly Boulder Nonlinear Systems). Hamamatsu has a wide selection of LC-SLMs, while Holoeye has the SLM with largest number of pixels, and Meadowlark offer slightly higher-performance optical specifications. Jenoptik have a linear LC-SLM array for femtosecond pulse shaping. Thorlabs and Santec also have some 2D LC-SLM models, with the latter also having a model designed specifically for the UV wavelength region. Cambridge Correlators manufacture a low-cost LC-SLM (~1k GBP) option with relatively lower specifications, though which is still highly suitable for optical trapping[21]. LC-SLM cost is usually linked to optical throughput and pixel number, with the highest resolution and best performing models priced the 20-30k GBP region.

It should be noted that deformable mirror membranes also provide rapid continuous phase modulation which is not polarization-sensitive, though at a much lower resolution than LC-SLMs. Such devices are typically expensive, though are more naturally suited to microscope aberration correction than LC-SLMs[14].

Summary of LC-SLM technology:

Positives:

- High pixel count displays (typically $>1000 \times 1000$, maximum known is 4160×2464 pixels for Holoeye GAEA-2)

- High-resolution phase control, typically ≥ 8 bits for 2π - 8π phase modulation range per pixel
- Some models are available with high fill factor (approaching 100%) and efficient optical throughput with anti-reflection coatings ($>90\%$ reflection).
- Can also be used for amplitude modulation with polarization optics.

Negatives:

- Polarization sensitivity
- High-end models are expensive (order of 20-30k GBP)
- Calculation of optical efficiency is more complex than for purely reflective (mirror-based) devices, as LC modulation involves polarization, reflection and diffraction effects.
- Undesirable higher-order diffraction effects from pixelated nature of device.

Amplitude modulation with digital micro-mirror devices (DMDs)

DMDs have emerged in recent decades from MEMS technology developed by Texas Instruments primarily for projector display purposes. Image contrast in such an application is controlled by rapidly switching micro-mirror tilt angle with variable duty cycle corresponding to grayscale control for each colour channel, with cycling through colour channels building up a time-averaged colour image. This technology has been exploited for binary and grayscale amplitude modulation in various areas of microscopy and imaging. Fill factors are typically high, and as the technology is mirror-based, total throughput can be above 90% for visible-NIR light. Thus applications for modulating weak Raman photons can be implemented with negligible degradation of the signal.

Texas instruments are the major manufacturer of DMD display devices. A low-cost DMD option is to modify a commercial projector product or evaluation board, such as the popular DLP Lightcrafter. Higher cost research-specific models also exist with direct access to the DMD display surface, with high-speed capability such as the Vialux V-700 with $>20\text{kHz}$ 1-bit array frame switching rates possible. Other than Texas Instruments, the Fraunhofer Institute for Photonic Microsystems also produce R&D MEMS mirror devices, including one-dimensional DMDs with up to 1 MHz frame rate.

Summary of DMD technology:

Positives:

- Widespread commercial availability resulting in low-cost options e.g. DLP Lightcrafter Evaluation development board available for approximately 500 GBP (requires some modification to access DMD display).
- Rapid refresh rates (typically several hundred Hz minimum) possible when using pre-determined low bit-depth patterns stored in on-device flash memory.
- Alternative display cable interfacing is simple to implement and allows standard video rate (60-120Hz) of arbitrary patterns generated in real-time
- Optical losses are minimal in the UV-VIS-NIR, as the technology is based on aluminium mirrors.
- High-resolution displays are available (up to 3840×2160 in current DLP660TE devices)

- Not polarization-sensitive

Negatives:

- Only amplitude modulation based on tilt-angle is possible
- Shallow mirror angles can make alignment difficult and often increases instrument size due to extra optics required. This is solved using integrated optics in commercial projector boards, which may not always be possible for prototyping in a lab on an optical table
- Pixelated spatial profile can generate unwanted higher-order diffraction effects
- Primarily designed for use in visible spectral region, though NIR-optimized models are emerging.

Examples of SLMs used in Raman spectroscopy

Uses of phase-modulation SLMs

Phase modulation SLMs are typically utilized in the excitation stage of a Raman instrument to modify the laser beam in various ways. While it may be possible to utilize modern LC-SLMs for modulating the detected Raman scattering, optical throughput is typically lower compared with mirror-based SLM devices, and laser photons are generally more readily available than Raman photons. Additionally, the effects of phase control on coherent monochromatic laser light offers additional effects which can be capitalized upon, such as holographic phase patterning for multiplexed beam steering. Here, we will discuss the various applications of LC-SLMs demonstrated in Raman spectroscopy instruments for enhanced control of the excitation laser source in some way.

Spatially controlled spontaneous Raman excitation

One of the biggest drawbacks in spontaneous Raman spectroscopy is the long acquisition times required for measurement, due to the inherently low Raman scattering cross-section for most materials of interest. The spontaneous Raman scattering intensity can be written as $I = \sigma NFD$ where σ is the Raman scattering cross section, N is the number of scatterers in the measurement volume, F is the source excitation flux, and D is the detection efficiency. Of these terms, F is the only parameter that can be readily adjusted in an experiment by increasing the laser power. However, this soon reaches a limit imposed either by available laser technology, or by sample damage threshold (particularly for life science applications). Thus, in order to further improve measurement times, smarter approaches to sampling must be considered.

Several strategies have been proposed for increasing the speed of Raman hyperspectral imaging, including multi-foci excitation, line-scanning and wide-field Raman imaging [10, 22, 23, 24]. One of the most direct approaches to such sampling is simply to create multiple parallelized laser excitation points for readout. Many approaches to this have been demonstrated, from using fixed optical elements such as lens arrays [25, 22, 26], to scanning galvo mirrors [27, 28, 29], and LC-SLMs [30, 31, 32]. The LC-SLM approach allows the most flexibility, and truly simultaneous excitation (opposed to temporal scanning of a single high-power beam), though also involves added computational

1
2
3 complexity and higher cost. Additionally, LC-SLMs generating multiple laser foci can also
4 be utilized for holographic optical trapping (HOT). The first use of LC-SLMs for optical
5 trapping in Raman spectroscopy was demonstrated by Qi and Shih, who were able to
6 measure polymer microparticles at 1,000 sampling points per second semi-randomly from
7 a $100 \times 100 \mu\text{m}^2$ field of view. Measurement of bacterial spores was also demonstrated at
8 a measurement rate of 2.5 sampling points per second. In this study, patterns were
9 generated such that sampling points did not overlap along one axis, as this would create
10 cross-talk on the CCD used for Raman spectroscopic measurement.
11
12

13
14 For measurements involving sampling points overlapping on one axis, cross-talk can be
15 avoided in several ways. Kong et al, demonstrated galvo mirrors for re-alignment through
16 a Raman CCD slit, however this time-shared scheme would result in a loss of efficiency if
17 an LC-SLM were used for power-shared excitation. In order to use completely power-
18 shared LC-SLM excitation efficiently, the group of Chan developed an electronically
19 controlled 4×5 block pattern matched to a slit array for Raman measurement from a multi-
20 focal array grid pattern. With knowledge of which slit patterns were used for measurement,
21 overlapping spectra could be computationally unmixed in post processing, which was
22 demonstrated for trapped arrays of polystyrene and PMMA microbeads.
23
24
25

26
27 **Figure 3. Examples of LC-SLMs for multi-point Raman spectroscopy. (a) Qi and**
28 **Shih[30, 31] initially demonstrated the use of an LC-SLM for programmable multi-point**
29 **illumination of laser sampling points for fast identification of micro-particles. (b) SLM of**
30 **an array of trapped particles overlapping in space, using an un-mixing protocol to retrieve**
31 **overlapped spectra[32].**
32
33

34
35 Multivariate hyperspectral imaging (MHI) based on compressive detection is an alternative
36 to achieve fast Raman mapping without using high laser power. MHI is a compressive
37 sampling strategy that utilizes a low-noise channel detector to simultaneously collect all
38 the photons transmitted by a multivariate optical filter. In cases when the CCD read-out
39 noise is the limiting factor, single channel detectors will have lower noise, and the
40 collection can be much faster than CCD-based spectral detection methods. The multivariate
41 filter plays a vital role in the MHI detection strategy, as it selects the photons to be collected,
42 and Raman spectra are later reconstructed based on the spectral shape using the
43 sequentially measured Raman photons. For detection of chemical mixtures, multiple
44 spectral patterns may be needed for classifying the binned photons. Thus the optical filter
45 should be rapidly switched to implement different spectral patterns. Spatial light
46 modulators are ideal for such an application, as they can be programmed to produce
47 variable filters with different spectral shapes with a rapid refresh rate ensuring fast
48 transitions between filter patterns. A compressed detection of Raman spectroscopy was
49 also realized using two types of SLM: LC-SLM [33] and DMD[34, 35, 36, 37]. Here we
50 will briefly introduce the LC-SLM based system, as the DMD-based system will be
51 presented in the amplitude-modulation SLM section of this review. Figure 4(a) shows the
52 diagram of the LC-SLM based compressive detection optics. A LC-SLM was placed at the
53 plane where a CCD camera located in a conventional Raman spectrometer. Raman
54 scattered light was dispersed by a volume holographic grating and directed on the SLM.
55
56
57
58
59
60

1
2
3 The SLM filter functions modulated the signal based on the polarization and reflected the
4 desired photons back into the detection path. The reflected signal was then collected by a
5 single channel detector, such as an avalanche photodiode (APD). Chemical imaging of an
6 aspirin and theophylline composite sample demonstrates the high-throughput of
7 multivariate hyperspectral Raman spectroscopy using compressive detection. The total
8 acquisition time of the chemical map shown in Figure 4(b) was 30 s (100×100 pixels).

9
10 A similar approach to spatially-encoded imaging was demonstrated by the group of K.
11 Dholakia, who used an LC-SLM to create spatial eigenmodes for effective wide-field
12 Raman imaging [38]. This approach used orthogonal 2D laser excitation patterns created
13 by an LC-SLM to excite Raman scattering and measured using a standard Raman
14 spectrometer. For sequential Raman measurements with different eigenmode patterns,
15 Raman hyperspectral images could be generated, with adjustable SNR and spatial
16 resolution depending on the number of sequential patterns utilized. Raman hyperspectral
17 imaging of polymers, pharmaceuticals and SERS probes was demonstrated with this
18 approach.
19

20 The same group also utilized the first-order diffracted light from an LC-SLM for Raman
21 measurement through a single multimode optical fiber [39]. The SLM allowed the
22 diffraction-limited excitation laser point to be spatially controlled in 3D at the distal end of
23 the fiber, as shown in Figure 5(a). This enabled point-scanned imaging, which was
24 demonstrated for polystyrene beads (Figure 5(b-d)), bacteria clusters, and pharmaceuticals.
25 This approach holds promise for endoscopic Raman hyperspectral imaging in biomedical
26 applications.
27
28
29
30

31 Figure 4. (a) Multivariate hyperspectral Raman imaging optical system using LC-LSM.
32 (b) Raman map of aspirin tablet with theophylline embedded (red), 100×100 pixels.
33
34
35

36 Figure 5. Raman hyperspectral imaging through a multimode fiber. (a) shows the
37 instrument setup. (b) shows example fiber background spectra and polystyrene sample
38 spectra. (c) shows a microscope image and (d) the corresponding point-scanning Raman
39 image of polystyrene beads through the fiber. [38]
40
41
42

43 Pulsed laser modulation in coherent Raman spectroscopy

44 Coherent Raman spectroscopy (CRS) techniques, in which pico- or femto-second pulsed
45 laser excitation is used to excite molecular vibrations via the third-order nonlinear
46 susceptibility, also have examples where SLMs have been utilized to improve the
47 instrument in some way. However, whereas LC-SLMs used in spontaneous Raman
48 spectroscopy are typically inspired by fluorescence or optical trapping, applications in CRS
49 typically borrow from other multiphoton microscopy or ultrafast pulse shaping techniques.
50 The two dominant CRS techniques are coherent anti-Stokes Raman (CARS) and stimulated
51 Raman scattering (SRS), both of which provide orders of magnitude speed up in
52 measurement acquisition times, though typically at the expense of spectral resolution and
53 increased complexity. Both techniques typically require multiple laser wavelengths to
54 generate a coherent vibrational state, and to probe this state[40].
55
56
57
58
59
60

1
2
3
4 The first demonstration of coherent Raman spectroscopy with spatial light modulators was
5 by group of Silberberg, who used an LC-SLM for pulse shaping[41]. While the refresh rate
6 of any SLM (or indeed most optical devices) is completely out of reach of ultrashort pulse
7 timescales, ruling out direct temporal modulation, spatial modulation of the dispersed pulse
8 spectrum can instead be used for pulse shaping. For a femtosecond pulse, modulation of
9 the pulse spectrum will result in the temporal profile of the pulse being modified (as the
10 two are linked via Fourier transformation). This is typically implemented as a $4f$ pulse
11 shaper, shown in Figure 6 (a), where the SLM is placed at the central position of a unity
12 magnification telescope with diffraction gratings at the front and back focal planes of the
13 telescope[12].
14
15

16
17 Femtosecond pulses are used for time-domain CARS, which is based on impulsive
18 stimulated Raman scattering, whereby all modes within the pulse bandwidth are excited by
19 a pump pulse, and CARS detection carried out using a time-varying probe pulse, generating
20 a CARS interferogram, which upon Fourier transformation produces a CARS spectrum.
21 The group of Silberberg et al utilized a pulse shaper to convert a single pulse into a pump
22 pulse and temporally varying probe pulse, simplifying the optical setup considerably. This
23 was possible using an LC-SLM in a pulse-shaping layout, to convert a single pulse into
24 two controllably temporally separated pulses, which were utilized as pump and probe for
25 the CARS process[41]. Using this approach, CARS spectra were able to be acquired in the
26 $400\text{-}800\text{cm}^{-1}$ spectral range, and CARS images of CH_2Br_2 liquid in a glass capillary plate
27 were demonstrated (Figure 6 (b)). Using the core idea of single-beam pulse shaping, many
28 other Raman-based excitation schemes have also been demonstrated including phase-
29 contrast[42] and single-beam SRS[43]. The group of M. Motzkus have also extended the
30 single-beam CARS approach by utilizing the attenuated edge of a pulse spectrum in the
31 LC-SLM pulse-shaper as a local oscillator for heterodyne amplification to increase
32 sensitivity by several orders of magnitude[44], and have also combined the pulse-shaping
33 CARS technique with other multiphoton imaging modalities[45]. Single-pulse two-
34 dimensional Raman spectroscopy was also demonstrated as shown in Figure 6 (d), where
35 pulses at three different excitation time-points were generated[46]. These methods utilize
36 the impulsive stimulated Raman process driven by short (femtosecond) but broadband laser
37 pulses to excite all vibrational modes within the pulse bandwidth. However, many CARS
38 and SRS instruments utilize two or more narrowband picosecond pulses to excite Raman
39 scattering from specific targeted vibrational modes. Halfway between is the use of both
40 femtosecond and picosecond pulses for multiplex SRS/CARS. Freudiger et al utilized an
41 SLM to tailor the femtosecond pulse spectrum in a multiplex SRS microscope, allowing
42 selective SRS excitations of vibrational modes within the pulse bandwidth as shown in
43 Figure 6 (c) [47]. A pulse shaping configuration was also used for programmable control
44 of a supercontinuum source, allowing shorter (femtosecond) pulse excitation for optimized
45 second/third harmonic generation and two-/three- photon fluorescence microscopy, while
46 picosecond pulses were programmed for CARS and SRS excitation[48]. Stranick et al. also
47 used LC-SLMs for phase-contrast CARS microscopy, where the SLM in order to create a
48 digital phase mask[49].
49
50

51 Phase-modulation with a deformable mirror membrane was demonstrated by Wright et al.
52 for adaptive aberration correction of a picosecond pulsed laser for deep-tissue CARS
53
54
55
56
57
58
59
60

1
2
3 microscopy[50]. In principle, LC-SLMs can be utilized for such aberration correction,
4 though deformable mirrors are better suited to this specific task as their phase modulation
5 is continuous, not pixelated [14].
6
7
8

9
10 Figure 6. Coherent Raman spectroscopy using LC-SLMs. (a) Schematic of the common
11 $4f$ pulse shaper used to spectrally modulate femtosecond laser pulses. (b) Single-pulse
12 CARS utilizing an LC-SLM pulse shaper to create a pump and temporally delayed probe.
13 Interferograms with inset spectra of methanol (left), CH_2Br_2 (middle) and $(\text{CH}_2\text{Cl})_2$
14 (right), and CARS spectroscopic images of CH_2Br_2 in a glass capillary plate [41]. (b)
15 Spectral tailoring of a femtosecond pulse for SRS imaging of multiple vibrational modes.
16 The LC-SLM is used with polarization for amplitude modulation of the spectrum, where
17 the spectral control is desired rather than temporal pulse control. This allowed imaging of
18 proteins (orange, left), oleic acid (blue, center) and stearic acid (magenta, right) within a
19 *C. Elegans* organism[47]. (d) Single-pulse 2D Raman spectroscopy, as an extension of
20 the idea of the single-pulse CARS in (a), where instead two temporally delayed probe
21 pulses are required for the Raman photon echo effect[46].
22
23
24
25

26 Uses of amplitude modulation SLMs

27 Raman spectrometer using a DMD and single-element detectors
28
29
30

31 Figure 7. Schematic of a DMD/PMT Raman spectrometer. [51]

32 Wagner *et al* first proposed a relatively inexpensive solution to build an optical
33 spectrometer using a digital micromirror device (DMD) and a single-element detector, such
34 as a photomultiplier tube (PMT) [52]. Quyen *et al* subsequently demonstrated the use of a
35 DMD/PMT spectrometer in Raman applications (schematic description shown in Figure
36 7(a)) [51]. Compared to typical Raman spectroscopy instruments, the major change in this
37 prototype is the use of a DMD as light modulator in the detection path to select Raman
38 light with specific wavelengths to the PMT. The dispersed Raman light from the grating
39 is directed onto the DMD, which consists of 1024×768 micro-mirrors that can be tilted \pm
40 12° relative to the normal of the display surface. The 1024 columns of micro-mirrors are
41 divided into 256 groups. By sequentially directing a group of mirrors towards the PMT
42 (with other mirrors directed in the opposing direction), a Raman spectrum can be obtained,
43 in a similar manner as with a Raman spectrometer based on a scanning monochromator.
44 To maintain good spectral resolution for the measured spectrum, only a few columns of
45 micromirrors are switched on at a time, though this leads to lengthy measurement time
46 when acquiring a full spectrum. It was later suggested that analytical precision could be
47 maintained if multiple characteristic peaks of a sample spectrum are measured at the same
48 time, which can be facilitated by the DMD/PMT configuration for multi-peak Raman
49 measurement. By taking the advantage of DMD/PMT Raman spectrometer, Quyen *et al*
50 demonstrated that wavelength selection sampling is almost as good as whole spectrum
51 recording in terms of qualitative analysis and quantitative analysis. Identification and
52 quantification of binary and ternary mixtures of chemicals were accurately achieved by
53
54
55
56
57
58
59
60

1
2
3 selective multi-peak sampling (see Figure 7(b)). Compared to whole spectrum analysis, the
4 total measurement was significantly shortened by skipping the recording of non-
5 informative data in the spectrum. However, *a priori* knowledge of the sample spectrum is
6 required for peak selection.
7

8
9 The acquisition speed can be further improved by combining DMD/PMT Raman
10 spectrometer with compressive detection approaches, which has been reviewed recently
11 [53]. The use of DMD to encode a Raman spectrum for measurement onto a single-pixel
12 detector was achieved by Ben-Amotz *et al* using binary filters, enabling rapid chemical
13 classification and simultaneous imaging of two chemical species in a sample. [34, 54] Since
14 the switching time of DMD mirrors can be as short as 10 μ s, multiple filters can be quickly
15 configured with varying integration times to achieve rapid Raman measurements. Rather
16 than sequentially select Raman bands on the DMD, rapid chemical classification was
17 implemented by differentiating the Raman scattering photons based on the filter
18 configuration and integration time for each filter set. The filters were generated based on
19 the pure Raman spectral features of the components of interest. In other words, training
20 spectra of the chemicals to be identified are required to construct accurate filters for
21 compressive detection. Similar to the DMD/PMT-based Raman spectrometer, full Raman
22 spectra of the samples were measured by DMD-based wavelength scanning. The obtained
23 training spectra were then used as an input to generate optimal filters. There are different
24 ways to generate filters. Digital and analogue compressive detection strategies have been
25 used for constructing filters. As DMD works only in a binary manner, digital filters are
26 more suitable. In contrast, LC-SLM works better with analogue detection strategy [33].
27
28
29
30

31 Later, the same group extended the DMD-based binary compressive detection strategy by
32 using two detectors to collect the Raman photons in two different channels [36]. With two
33 detectors, all Raman photons can be collected by using a pair of complementary binary
34 filters that direct photons toward either of the detectors. The optical layout is slightly
35 different from that which uses a single detector, as the two detectors are facing the $\pm 12^\circ$
36 position relative to the DMD, respectively. By using complementary binary filters, the
37 number of measurements can be reduced compared to single detector strategy. Moreover,
38 the most significant advantage of using two detectors is that when only two significant
39 components to be classified or quantified, only a single pair of complementary filters is
40 needed, and there is no dead-time or delay due to switching the DMD mirrors. For
41 classifying an acetone and benzene liquid mixture, the total measurement time was 10% of
42 the single detector approach. Raman imaging of a two-component sample mixture with
43 600×600 μ m area (240×240 pixels) was finished in 4 s, demonstrating the capability of
44 DMD/PMT-based compressive detection for fast hyperspectral Raman imaging.
45
46
47

48 More recently, Scotte *et al* compared the speed performance of DMD/PMT-based
49 compressive Raman imaging to two state-of-the-art hyperspectral Raman imaging systems
50 [37]. The configuration of the DMD/PMT-based system was similar to the one shown in
51 Figure 7(a), while the other two instruments using a CCD or an EMCCD. By imaging
52 powder mixture samples mimicking micro-calcifications relevant for breast cancer
53 diagnosis, the authors showed that the DMD/PMT-based compressive system allows $100\times$
54 and $10\times$ faster acquisition speed than the CCD- and EMCCD-based systems, respectively.
55
56
57
58
59
60

1
2
3
4
5
6 Figure 8. (a) Concept of compressed Raman imaging. The Raman scattered light is firstly
7 encoded with a binary mask on a DMD, then imaged by a spectrometer. The latter
8 spatially shears the image based on the spectral content. Last, a reconstruction algorithm
9 based on the encoding mask recovers hyperspectral images of the original scene. (b)
10 Experimental setup. (c) Recovered Raman image compared to bright-field image.[35]
11

12 While DMD/PMT-based compressive detection provides a means to increase the speed for
13 chemical classification and imaging, the original spectral information is lost during the
14 computational analysis, as the latter is performed before data acquisition. Thompson *et al*
15 [35] reported a technique of single-shot compressed hyperspectral Raman imaging by
16 utilizing a combination of DMD and spectrometer to achieve spatio-spectral compressive
17 detection, where full spectral information can be retrieved after reconstruction. Instead of
18 a single-channel detector, a spectrometer consisting of a grating and a CCD camera was
19 used for detection. Figure 8(a) shows the concept of this approach to compressed Raman
20 imaging. Similar to DMD/PMT-based compressive detection, here the DMD was used to
21 encode a binary mask onto the image of the sample. The grating in the spectrometer then
22 sheared the spectral information in the spatial domain, and the CCD detector captured the
23 full spectral information at each pixel of the acquired image. Afterwards, a full-resolution
24 hyperspectral data cube was recovered from the encoded two-dimensional CCD image.
25 Hyperspectral Raman image of barium sulfate (BaSO_4) powder on an
26 olytetrafluoroethylene (PTFE) block was successfully recovered from a compressed data.
27 The latter was obtained in a single acquisition with CCD integration time of 5 s. Compared
28 to the aforementioned DMD/PMT-based compressive detection strategy, speed may not be
29 an advantage for DMD/CCD-based compressed sensing, but the key advantage lies in the
30 fact that full spectral information is reserved, and no prior knowledge of the sample is
31 needed for constructing the encoding mask.
32
33
34
35

36 All examples of DMD-based sensing above utilized spontaneous Raman spectroscopy,
37 however broadband SRS measurements have also been demonstrated recently utilizing a
38 DMD with a single-pixel detector for Hadamard-based spectral compressive sensing[55].
39
40
41

42 DMD-based spatially offset Raman spectroscopy

43 Non-invasive chemical depth-profiling of materials is of high interest to a broad range of
44 applications, such as pharmaceutical industry, security, food quality inspection and non-
45 invasive medical diagnosis. Confocal Raman spectroscopy is a popular choice for non-
46 invasive spectral depth-profiling, but the depth range is usually limited to the order of
47 micro-meters. Matousek *et al* [56] introduced a technique called spatially-offset Raman
48 spectroscopy (SORS) that can measure subsurface chemical information from materials
49 eliciting high levels of light scattering. SORS is based on the multiple diffuse scattering of
50 light in turbid media, and involves laterally offset detection relative to the laser excitation
51 spot on the sample.
52
53

54 The implementation of SORS is usually achieved with fiber optics bundles, where optical
55 fibers are arranged in one or more concentric circles to realize spatial offsets for Raman
56
57
58
59
60

1
2
3 photon collection. Since the fibers are fixed in the bundles, these probes lack the ability to
4 change the spatial offsets. Therefore, the range of sample depths is limited by the radii of
5 the concentric circles. Inverse SORS improves the flexibility by delivering the excitation
6 beam with an annular profile at the sample, and detecting the Raman photons through the
7 optical fibers at the center of the probe[57]. Some other methods have also been proposed
8 to achieve adjustable spatial offsets for SORS measurement, but either involves
9 modifications of the mechanical parts in the optical system[58], or have low optical
10 throughput[59].

11
12
13 Liao *et al* recently proposed a novel design to implement SORS by using a DMD added to
14 a conventional Raman spectrometer[60]. The system enables efficient and flexible
15 collection of SORS signals, with software-configurable selection of the spatial offsets,
16 requiring no changes to the optical system or mechanical adjustment. Single-point, annular
17 and multi-offset collection geometries can be easily achieved by altering the pattern
18 displayed on the DMD.
19
20

21
22 A schematic of the DMD-SORS system is shown in Figure 9(a). The excitation laser is
23 guided into a microscope and focused on to the sample as in a conventional backscattering
24 Raman instrument. Backscattered Raman photons are collected by the objective and
25 focused onto a DMD by a lens. The DMD is placed at a sample-conjugate plane to serve
26 as the spatial offsets controller for SORS measurement, as well as slit/pinhole for the
27 Raman spectrometer.
28
29
30
31

32 Figure 9. (a) Schematic of SORS optical system using DMD as a computer-controlled
33 spatially offset mask. (b) single-offset semi-annulus collection geometry with high
34 efficiency. (c) multiple-offset collection geometry with low efficiency. [55] (d) DMD-
35 SORS detection of mineralization through chicken skin and tissue engineering scaffolds
36 [60].
37
38

39
40 The DMD is at the core of this SORS system, as the spatial offsets are implemented by
41 displaying binary images with annular-like collection patterns. As illustrated in Figure 9(b),
42 a semi-annular pattern consisting of seven collection points is displayed on the DMD. Each
43 point is a group of tiled DMD mirrors ('on' state) that guide the Raman signal toward the
44 spectrometer, while all the black area are mirrors in 'off' state where light is rejected from
45 the spectrometer. These collection points are equally distant from the central point that
46 corresponds to the conjugated point of the laser on the sample, so that an averaged SORS
47 spectrum can be obtained by horizontally shifting and vertically overlapping the stripes of
48 acquired CCD Raman image. The collection points were arranged in a way that there was
49 no more than one point in 'on' state horizontally, so that the crosstalk of Raman spectra on
50 the CCD can be prevented. Vertical gaps of 10 micro-mirrors were retained for the same
51 reason. The actual spatial offset on the sample is determined by the radius of the semi-
52 circle, S , displayed on DMD, and the focal lengths, f_0 and f_m , of the focusing lens in front
53 of the DMD and the microscope objective, respectively. This concentric collection
54 geometry can provide collection efficiency up to $\sim 25\%$, comparable to that of optical fibre
55
56
57
58
59
60

1
2
3 bundles with tightly-packed collection fibers. Moreover, the key advantage of DMD-SORS
4 system lies in the fact that the values of spatial offset can be easily changed, as the binary
5 image on DMD is software-configured, and requires no movable mechanical parts. The
6 range of spatial offsets is only restricted by the dimension of active area of the DMD and
7 the CCD sensor. For the initial demonstration, values of spatial offset could be readily
8 selected in the range of 0 – 1 mm using a 2× microscope objective with 90 mm focal length.
9 The capability and flexibility of the DMD-SORS was demonstrated by measuring a two-
10 layer structure consisting of a PMMA sheet as top layer and PS sheet as bottom layer. From
11 Figure 9 (b) we can see, as the value of spatial offset increased from 0 to 1 mm, the Raman
12 band at $\sim 809\text{ cm}^{-1}$ assigned to PMMA decreased gradually, while the intensity of Raman
13 bands assigned to PS increased.
14
15

16
17 To further demonstrate the flexibility of DMD-based SORS, measurements with
18 simultaneous multiple offsets were carried out. A collection geometry using a v-shaped
19 pattern was used, as the points in each arm represent different spatial offsets from the laser
20 excitation position. As depicted in Figure 9 (c), 8 SORS spectra with different offsets can
21 be obtained from the two-layer polymer sample in a single acquisition. Ratiometric data of
22 Raman intensity clearly shows that there was a trend of intensity increase from the bottom
23 layer as the spatial offset increased from 0-1 mm. Since there was only two collection
24 points for each offset, the collection efficiency was reduced compared to concentric semi-
25 circle geometry, led to lower signal to noise ratio of the spectra.
26
27

28
29 Later the authors investigated the feasibility of using DMD-based SORS for non-
30 destructive characterization of bone tissue engineering scaffolds[61]. Raman spectroscopy
31 is a powerful technique for characterization of tissue engineering scaffolds and cells [62,
32 63]. However, measuring molecular signals from the inner parts of the scaffolds is
33 hampered by the high level of optical scattering elicited by these materials. SORS
34 measurements on 3D tissue engineering scaffolds show that hydroxyapatite (HA) can be
35 reliably detected up to depths of 0 – 2.3 mm. Furthermore, SORS detection of HA was also
36 possible when the scaffolds were covered by a 1 mm thick fresh chicken skin (see Figure
37 9(d)). These proof of principle experiments demonstrate the feasibility of using DMD-
38 based SORS for monitoring the in-vitro and in-vivo mineralization of bone tissue
39 engineering scaffolds.
40
41

42 DMD/SPAD-based Time-Gated Raman Spectroscopy

43 Laser-induced fluorescence emission is a major problem in Raman spectroscopy
44 measurements of pigmented samples, including many biological samples. A variety of
45 fluorescent components in tissue give a strong and broad emission that swamp the weak
46 Raman signal. Various strategies have been used to suppress the fluorescence background
47 in the Raman spectra. Laser-induced tissue fluorescence is often spectrally active in the
48 UV and visible range, so it can be effectively avoided in Raman measurement by using an
49 excitation laser with wavelength in the near-infrared (NIR), e.g. 785 nm. However, in
50 many cases, the use of 785-850 nm lasers is still not sufficiently effective when it comes
51 to pigmented biological samples. An excitation wavelength further in the NIR, e.g. 1064
52 nm, can be used to avoid auto-fluorescence, but requires different components for the
53 optical system, in particular InGaAs or Ge CCD detectors. The dark current and read-out
54
55
56
57
58
59
60

1
2
3 noise levels of these detectors are several orders of magnitude higher than the Si CCD used
4 when using lasers with wavelengths shorter than 850 nm. In addition, increasing the
5 wavelength of excitation laser also reduces the efficiency of Raman scattering (Raman
6 efficiency $\sim \lambda^{-4}$). The fact that Raman scattering has a much shorter lifetime (less than a
7 picosecond) than fluorescence emission (range from a few nanoseconds to tens of
8 nanoseconds), makes it possible for separating Raman photons from fluorescence
9 background in the time-domain using time-gating methods.

10
11 Recently, Corden *et al* reported time-gated Raman spectroscopy using a single photon
12 counting detector with a DMD for spectral filtering and multiplexing[64]. The optical
13 system is depicted in Figure 10(a). A pico-second pulsed laser with 60 MHz repetition rate
14 at 775 nm wavelength was employed as excitation source. Similar to previously introduced
15 DMD/PMT-based Raman spectrometer, a combination of a spectrometer and a DMD was
16 used for selecting the photons corresponding to the Raman bands of interest. The
17 collimated Raman scattered and fluorescence photons from the spectrometer were directed
18 onto the DMD, where columns of mirrors were switched 'on' and 'off' to select the desired
19 Raman bands. The selected photons were then fed into a single photon avalanche diode
20 (SPAD) after spectral recombining using two prisms. The SPAD separated the Raman and
21 fluorescence in the time domain, achieving in this way a high level of fluorescence
22 background suppression in the Raman spectra.
23
24
25
26
27
28

29 Figure 10. (a) Schematic of DMD/SPAD-based time-gated Raman spectroscopy system.
30 (b) Bright-field image of the Tylenol and stilbene powder on a glass coverslip (mapping
31 area $120\mu\text{m} \times 120\mu\text{m}$). (c) Time-gated spectra of stilbene (circle) and Tylenol (triangle).
32 The bands used for multiplexing are highlighted. (d) Time-gated Raman spectra at the
33 same locations after the addition of the fluorescing dye on top of the sample. (e) Time-
34 gated Raman maps acquired in the DMD multiplexing mode corresponding to the
35 Tylenol (left) and stilbene (right) bands. Acquisition times: 3 minutes for stilbene maps,
36 27 minutes for the Tylenol maps. (f) Combined pseudo-color Raman map: Tylenol
37 (purple) and stilbene (green); time-gate was 120ps for Tylenol, and 160ps for stilbene,
38 total time: 30 minutes. [64]
39
40

41 To demonstrate the capability of the system for time-gated Raman mapping, a mixture of
42 trans-stilbene and Tylenol powder was covered with a fluorescing dye solution was used
43 (Figure 10(b)). Full Raman spectra of pure trans-stilbene and Tylenol were first acquired
44 by notch DMD scanning, respectively, in order to identify the Raman bands that can be
45 used to discriminate between the two materials, as shown in Figure 10(c-d). Then, the
46 powder mixture with covered by the fluorescing dye solution was imaged by raster
47 scanning. In a first scan shown in Figure 10(e), the columns of DMD mirrors were set to
48 select and multiplex the Raman bands corresponding to trans-stilbene. For the second scan,
49 a different group of mirrors were used for selection of Raman photons from Tylenol.
50 Raman photons were separated from the fluorescence background using a time-gate of 160
51 ps. Figure 10(f) shows the pseudo-color Raman map corresponding to the mixture powder
52 sample, demonstrating that the fluorescence background was effectively suppressed, and
53 the two components in the powder were identified. While the total imaging time is on a
54 similar time-scale to standard Raman point-mapping (30 minutes for a 40×40 pixels image:
55
56
57
58
59
60

0.9 s dwell time), the SNR enhancement in the presence of strong fluorescence enables the measurement of previously difficult or even impossible-to-measure samples.

Uses of multiple SLM devices

Multi-focal RMS

Using a high laser power to create multi-foci for excitation of Raman scattering is a promising strategy to improve the acquisition speed of Raman imaging. In principle, the acquisition time can be decreased by a factor equal to the number of laser foci. While various optical elements have been used for generation fixed patterns of multi-foci, such as microlens array[25], diffractive optical elements [65] and galvomirrors [28], Sinjab *et al* developed such a multi-foci Raman micro-spectroscopy system utilizing LC-SLM and DMD[10]. The schematic description of the instrument is shown in Figure 11(a). The LC-SLM generates desired pattern of laser foci, and the DMD in the detection path functions as a software configurable reflective pinhole array. Both the SLM and DMD are synchronized and controlled through software, any changes of the position and number of the laser foci in real time can be rapidly achieved without requiring any hardware alteration.

Figure 11. (a) Schematic description of multi-foci Raman system using SLM and DMD. (b) Simultaneous multi-foci Raman measurements on skin tumor resection for cancer diagnosis.[10]

The authors tested the feasibility of multi-foci RMS for fast cancer diagnosis. RMS has been demonstrated for measuring chemical differences between healthy tissue and tumor with high sensitivity and specificity[66]. However, Raman imaging of large tissue sample is often a long process, makes it unsuitable for intro-operative diagnosis. A multimodal spectral imaging (MSI) combining selective sampling Raman spectroscopy and auto-fluorescence imaging was used to image large tissue samples to detect residual tumour cells[67]. Tissue autofluorescence (AF) imaging were first used to eliminate the non-suspicious area, the remaining part was then used to select and prioritize the sampling points for Raman measurement, with an optimized MSI algorithm allowing high diagnosis accuracy while minimizing the number of Raman acquisition[68]. With this sampling strategy, the time for cancer detection of tissue resections can be effectively shortened, and diagnosis of basal cell carcinoma of surgically resected skin tissue was achieved in 30 minutes[69]. To further increase the speed and diagnosis accuracy, multi-foci RMS was employed for cancer detection after generating sampling points from AF imaging. A CW Ti:Sapphire laser (3 W output, <1 W total at sample) with 785 nm wavelength was used to generate multi-foci created by the LC-SLM, and Raman spectra from six sampling points of skin tissue resections were acquired simultaneously, as shown in Figure 11(b). Diagnosis of large skin tissue samples ($\sim 1 \text{ cm}^2$) obtained in surgery was achieved in 11 minutes, indicating the speed advantage of multi-foci RMS. This initial study demonstrates the potential of this approach to enable intra-operative use of Raman spectroscopy for cancer surgery, in particular for cases where the size of the resected tissue can be as large as several

centimeters, as is in the case of breast cancer [70, 71]. This instrument approach could also be utilized for other selective point-sampling approaches[72, 73].

Multi-focal Raster Scan Imaging

While multi-focal Raman scanning can improve the speed of Raman mapping, cross-talk caused by overlapping laser beams and diffuse scattering of Raman photons reaching the detector can degrade the depth discrimination compared to single-beam confocal Raman microscopy. The SLM/DMD multi-foci Raman system provided the flexibility to investigate the depth-discrimination and speed performance of multi-foci Raman hyperspectral imaging[11]. Multi-focal patterns with different periods were readily realized and used to study the effects of laser foci overlap and Raman signal cross-talk on spectral depth discrimination.

Figure 12. SLM/DMD-based multi-foci confocal Raman imaging. (a) SLM/DMD patterns and corresponding Raman CCD images used for multifocal hyperspectral Raman imaging. (b) Optical sectioning by multi-foci Raman imaging of diphenylalanine micro-tubes.[11]

To investigate the influence of the distance between adjacent laser foci on the depth discrimination of multi-foci confocal Raman system, optical configuration with different distance-to-size ratio (R) were compared. The parameter R refers to the ratio between the distance between the centres of adjacent pinholes D , and the diameter of the pinhole S (Figure 12 (a)). Nine laser foci configuration with R from 2 to 16 were easily achieved without altering any optical components in the system, as the SLM/DMD provided the flexibility to modify the number, location and spacing among the laser foci. Figure 12 (a) shows the Raman CCD images using different laser foci configuration. After optimizing the configuration for fast spectral Raman imaging with good depth discrimination, a 9-beam, $R = 8$ configuration was used for hyperspectral imaging of micro-materials and cells. Figure 12 (b) shows an example of optical sectioning of diphenylalanine micro-tubes, showing good depth discrimination and speed performance highlighting the advantage of SLM/DMD-based multi-foci Raman imaging.

Laser tweezers Raman spectroscopy

Using the LC-SLM/DMD combination in the previous section, but coupled with a much higher NA objective, simultaneous multi-point holographic optical trapping (HOT) and Raman spectroscopy could be carried out[74]. The LC-SLM used was controlled by RedTweezers software developed by Bowman et al.[20], which utilized GPU processing to provide high-speed calculation of phase holograms ($>60\text{Hz}$), allowing real-time and interactive optical manipulation of microparticles. Sinjab et al extended this to incorporate Raman spectroscopy by using the same trapping beams for excitation, and collecting the backscattered Raman light through a dichroic mirror, and imaging the sample plane onto a DMD device to allow the spatial filtering before entering the spectrograph. The performance of the instrument (acquisition times, spatial resolution, spectral resolution etc.) was found to be comparable to single-beam Raman microscopes, which allowed

dynamic Raman micro-spectroscopy measurements to be carried out, as shown in Figure 13(a). Here, four polystyrene microparticles were manipulated by the user in software in real-time, whilst Raman spectra were acquired and microscope camera images were acquired (microscope light switched on during first 90s). The read-out was limited to 10Hz (4x10 spectra per second) by the spectrometer shutter.

Figure 13. Holographic optical trapping Raman micro-spectroscopy. (a) shows video frames and time-course Raman spectra dynamic manipulation-measurement experiment of four trapped 3 μ m polystyrene beads in four regions of the FOV, from which Raman spectra were acquired at 10Hz (total 40 spectra per second). (b) shows multiple trapped cells in different flexible configurations and controlled excitation power to avoid damage. [74]

Using the HOT-Raman micro-spectroscopy instrument, it was possible to trap and manipulate various cell types, while simultaneously measure their Raman spectra, as shown in Figure 13(b). The sensitivity of particular live cells to persistent laser irradiation was investigated using time-course measurements, by observing changes in the raw data baseline and changes in Raman bands at various laser excitation powers to determine the damage thresholds.

To demonstrate the unique capability of this approach, the HOT-Raman instrument was used to investigate the spectral changes in human T and dendritic cells during the formation of an immune synapse. Multiple floating T-cells could be optically manipulated into contact with an adherent dendritic cell (DC). After attachment, HOT-Raman spectroscopy was utilized to measure at specific spatial locations of the interacting cell system, to determine differences between junctions and the main cellular bodies. The Raman difference spectra suggested increased protein content at the junction, agreeing with previous studies based on Raman hyperspectral imaging[75].

Future directions & conclusion

We have reviewed the use of SLM devices within the broad field of Raman spectroscopy, highlighting a multitude of novel instrumentation approaches and their various applications. Such devices have many advantages, as they allow real-time software control, increased instrument flexibility, options for automation, and allowing digital signal processing techniques applied to light in spatial, spectral and temporal domains.

LC-SLMs are particularly useful for providing a flexible way of controlling the spatial and temporal properties of the laser excitation in spontaneous and coherent Raman spectroscopies. Examples of this ranged from generating multi-point spontaneous Raman excitation for improved measurement times, to shaping pulsed laser beams to allow coherent Raman spectroscopy using single laser sources.

LC-SLMs have not often been utilized for modulation of Raman scattered photons, likely due to the expected losses in an already Raman weak signal. However, the demonstration of an LC-SLM for compressive sensing by modulating the Raman spectrum shows that high-performance LC-SLMs have sufficient throughput to be useful for applications in

1
2
3 Raman spectroscopy[33]. This feasibility of using an LC-SLM for modulating Raman
4 signals may lead to novel applications in the future.
5

6
7 Other phase modulation devices such as deformable mirrors, which have thus far not been
8 widely utilized in Raman spectroscopy, may offer improvement of aberration
9 correction[14], which has been demonstrated to be useful for focusing within highly
10 scattering tissue for CARS[50]. These devices may also be useful for correcting aberrations
11 in spontaneous Raman hyperspectral imaging on high-background substrates, where it has
12 been shown that spherical aberrations can lead to increase contamination of the Raman
13 spectrum due to the shot noise caused by the Raman photons generated in the substrate
14 even after background subtraction[76].
15

16
17 DMDs have typically been utilized in the detection stages of Raman instruments, as their
18 high reflectivity and fill factor facilitate the necessarily high throughput required for
19 detecting the weak spontaneous Raman scattering signal. Examples included spectral
20 modulation of the Raman signal for computational, compressive, or fluorescence-rejection
21 purposes and sample-conjugate spatial modulation for multi-confocal and spatially-offset
22 Raman measurements.
23

24
25 DMDs could also be utilized for modulation of the Raman excitation laser, for example in
26 Hadamard-encoded imaging, though this would result in significant losses during the
27 patterning process which LC-SLM approaches could reduce. One possibility may include
28 dynamic range enhancement for wide-field Raman excitation, as has been demonstrated
29 for bright-field imaging[77].
30

31
32 Another potential use of DMDs is for periodic shadowing spectroscopy, which is
33 essentially spatial lock-in detection for removal of undesirable stray light. This involves
34 periodic amplitude modulation of light being analysed by a spectrometer along the spatial
35 (slit) axis, with the signal retrieved via a lock-in procedure using the known patterning
36 process as the reference waveform. This was initially demonstrated for a variety of
37 spectroscopy techniques (including CARS) using a fixed Ronchi grating for patterning,
38 and later for emission spectroscopy using a DMD with additional dynamic range
39 enhancement[78, 79]. The latter DMD approach could also be utilized for Raman
40 spectroscopy, and could also be combined with other DMD-based methods as only one
41 spatial axis is required for the shadowing pattern. Spatial patterning can also be used for
42 structured illumination microscopy [80], which has also been demonstrated in Raman
43 micro-spectroscopy using a fixed patterned line illumination[81], which could also use
44 either an LC-SLM or DMD in principle allowing enhanced flexibility in pattern generation.
45
46
47

48 While the focus of this review has been on Raman spectroscopic applications, SLMs may
49 also be of use to infra-red vibrational spectroscopy, particularly due to the limitations of
50 2D detectors in this spectral region. DMDs in particular have been utilized beyond their
51 optical specifications for video-rate single-pixel vibrational imaging of gas leaks at 1500
52 nm [82] and for combined visible/NIR single-pixel microscopy [83]. With the emergence
53 of novel high-power IR sources, it can be expected that many more possibilities will
54 emerge in this direction, particularly as SLM devices operational in the NIR-MIR are
55
56
57
58
59
60

developed further[84]. In addition to SLM optical properties, increased update speeds for pulse-shaping applications would be desirable for some Raman applications where rapid pulse control is required, such as Fourier-transform CARS, which is currently achieved by much faster mechanical scanning processes [85, 86].

In summary, SLM devices have been shown to augment many existing Raman instrument modalities, enhancing several applications in the spatial and spectral domains in the process. In some cases, SLMs have even allowed Raman instrumentation concepts which would otherwise not have been possible at all.

References

- [1] S.B. Dierker, C.A. Murray, J.D. Lefrange, N.E. Schlotter. "Characterization of Order in Langmuir-Blodgett Monolayers by Unenhanced Raman Spectroscopy". *Chem. Phys. Lett.* 1987. 137(5):453–457.
- [2] C.J. Frank, D.C.B. Redd, T.S. Gansler, R.L. McCreery. "Characterization of Human Breast Biopsy Specimens with Near-IR Raman Spectroscopy". *Anal. Chem.* 1994. 66(3):319–326.
- [3] B. Yang, M.D. Morris, H. Owen. "Holographic Notch Filter for Low-Wavenumber Stokes and Anti-Stokes Raman Spectroscopy". *Appl. Spectrosc.* 1991 45(9):1533–1536.
- [4] M. Delhaye, P. Dhamelincourt. "Raman Microprobe and Microscope with Laser Excitation". *J. Raman Spectrosc.* 1975. 3(1):33–43.
- [5] R.M. Stöckle, Y.D. Suh, V. Deckert, R. Zenobi. "Nanoscale Chemical Analysis by Tip-Enhanced Raman Spectroscopy". *Chem. Phys. Lett.* 2000. 318(1-3):131–136.
- [6] G.J. Puppels, F.F.M. De Mul, C. Otto, J. Greve, M. Robert-Nicoud, D.J. Arndt-Jovin, T.M. Jovin. "Studying Single Living Cells and Chromosomes by Confocal Raman Microspectroscopy". *Nature*, 347(6290):301, 1990.

- 1
2
3 [7] D.W. Shipp, F. Sinjab, I. Notingher. “Raman Spectroscopy: Techniques and
4 Applications in the Life Sciences”. *Adv. Opt. Photonics*. 2017. 9(2):315–428.
5
6
7
8 [8] L.A. Nafie. “Recent Advances in Linear and Non-Linear Raman Spectroscopy. Part
9 XI”. *J. Raman Spectrosc.* 2017. 48(12):1692–1717.
10
11
12 [9] M. Reicherter, T. Haist, E.U. Wagemann, H.J. Tiziani. “Optical Particle Trapping
13 with Computer-Generated Holograms Written on a Liquid-Crystal Display”. *Opt.*
14 *Lett.* 1999 24(9):608–610.
15
16
17
18 [10] F. Sinjab, K. Kong, G. Gibson, S. Varma, H. Williams, M. Padgett, I. Notingher.
19 “Tissue Diagnosis using Power-Sharing Multifocal Raman Micro-Spectroscopy and
20 Auto-Fluorescence Imaging”. *Biomed. Opt. Express* 2016. 7(8):2993–3006.
21
22
23 [11] Z. Liao, F. Sinjab, H.M. Elsheikha, I. Notingher. “Optical Sectioning in Multifoci
24 Raman Hyperspectral Imaging”. *J. Raman Spectrosc.* 2018. 49(10):1660–1667.
25
26
27 [12] A.M. Weiner. “Femtosecond Pulse Shaping using Spatial Light Modulators”. *Rev.*
28 *Sci. Instrum.* 2000. 71(5):1929–1960.
29
30
31 [13] G.D. Love. “Wave-Front Correction and Production of Zernike Modes with a
32 Liquid-Crystal Spatial Light Modulator”. *Appl. Opt.* 1997. 36(7):1517–1524.
33
34
35 [14] M.J. Booth. “Adaptive Optical Microscopy: the Ongoing Quest for a Perfect Image”.
36 *Light Sci. Appl.* 2014. 3(4):e165.
37
38
39 [15] M.F. Duarte, M.A. Davenport, D. Takhar, J.N. Laska, T. Sun, K.F. Kelly, R.G.
40 Baraniuk. “Single-Pixel Imaging via Compressive Sampling”. *IEEE Signal*
41 *Processing Magazine*. 2008. 25(2):83–91.
42
43
44 [16] V. Studer, J. Bobin, M. Chahid, H.S. Mousavi, E. Candes, M. Dahan. “Compressive
45 Fluorescence Microscopy for Biological and Hyperspectral Imaging”. *Proc. Natl.*
46 *Acad. Sci. U. S. A.* 2012. 109(26):E1679–E1687.
47
48
49
50
51
52
53
54
55
56
57
58
59
60

- 1
2
3 [17] Q.S. Hanley, P.J. Verveer, T.M. Jovin. "Spectral Imaging in a Programmable Array
4 Microscope by Hadamard Transform Fluorescence Spectroscopy". *Appl. Spectrosc.*
5 1999. 53(1):1–10.
6
7
8
9 [18] G.M. Gibson, M. Dienerowitz, P.A. Kelleher, A.R. Harvey, M.J. Padgett. "A Multi-
10 Object Spectral Imaging Instrument". *J. Opt.* 2013. 15(8):085302.
11
12
13 [19] G. Thalhammer, R.W. Bowman, G.D. Love, M.J. Padgett, M. Ritsch-Marte.
14 "Speeding up Liquid Crystal SLMs using Overdrive with Phase Change Reduction".
15 *Opt. Express* 2013. 21(2):1779–1797.
16
17
18 [20] R.W. Bowman, G.M. Gibson, A. Linnenberger, D.B. Phillips, J.A. Grieve, D.M.
19 Carberry, S. Serati, M.J. Miles, M.J. Padgett. "Red Tweezers": Fast, Customisable
20 Hologram Generation for Optical Tweezers". *Comput. Phys. Commun.* 2014.
21 185(1):268–273.
22
23
24 [21] R. Bowman, V. D'Ambrosio, E. Rubino, O. Jedrkiewicz, P. Di Trapani, M.J.
25 Padgett. "Optimisation of a Low Cost SLM for Diffraction Efficiency and Ghost
26 Order Suppression". *Eur. Phys. J.: Spec. Top.* 2011. 199(1):149–158.
27
28
29 [22] S. Yabumoto, H.-o. Hamaguchi. "Tilted Two-Dimensional Array Multifocus
30 Confocal Raman Microspectroscopy". *Anal. Chem.* 2017. 89(14):7291–7296.
31
32
33 [23] J. Qi, W.-C. Shih. "Performance of Line-Scan Raman Microscopy for High-
34 Throughput Chemical Imaging of Cell Population". *Appl. Opt.* 2014. 53(13):2881–
35 2885.
36
37
38 [24] D. Wei, S. Chen, Y.H. Ong, C. Perlaki, Q. Liu. "Fast Wide-Field Raman
39 Spectroscopic Imaging Based on Simultaneous Multi-Channel Image Acquisition
40 and Wiener Estimation". *Opt. Lett.* 2016. 41(12):2783–2786.
41
42
43 [25] M. Okuno, H.-o. Hamaguchi. "Multifocus Confocal Raman Microspectroscopy for
44 Fast Multimode Vibrational Imaging of Living Cells". *Opt. Lett.* 2010. 35(24):4096–
45 4098.
46
47
48
49
50
51
52
53
54
55
56
57
58
59
60

- 1
2
3 [26] Y. Kumamoto, Y. Harada, H. Tanaka, T. Takamatsu. "Rapid and Accurate
4 Peripheral Nerve Imaging by Multipoint Raman Spectroscopy". *Sci. Rep.* 2017.
5 7(1):845.
6
7
8
9 [27] L. Kong, P. Zhang, J. Yu, P. Setlow, Y.-q. Li. "Rapid Confocal Raman Imaging
10 using a Synchro Multifoci-Scan Scheme for Dynamic Monitoring of Single Living
11 Cells". *Appl. Phys. Lett.* 2011. 98(21):213703.
12
13
14
15 [28] L. Kong, M. Navas-Moreno, J.W. Chan. "Fast Confocal Raman Imaging using a 2-D
16 Multifocal Array for Parallel Hyperspectral Detection". *Anal. Chem.* 2015.
17 88(2):1281–1285.
18
19
20 [29] M. Navas-Moreno, J.W. Chan. "Improving the Imaging Speed of 1064 nm
21 Dispersive Raman Microscopy with Multifocal Patterned Detection". *Opt. Lett.*
22 2017. 42(1):37–40.
23
24
25 [30] J. Qi, W.-C. Shih. "Parallel Raman Microspectroscopy using Programmable
26 Multipoint Illumination". *Opt. Lett.* 2012. 37(8):1289–1291.
27
28
29 [31] J. Qi, J. Li, W.-C. Shih. "High-Speed Hyperspectral Raman Imaging for Label-Free
30 Compositional Microanalysis". *Biomed. Opt. Express* 2013. 4(11):2376–2382.
31
32
33 [32] L. Kong, J. Chan. "A Rapidly Modulated Multifocal Detection Scheme for Parallel
34 Acquisition of Raman Spectra from a 2-D Focal Array". *Anal. Chem.* 2014.
35 86(13):6604–6609.
36
37
38 [33] B.M. Davis, A.J. Hemphill, D.C. Maltas, M.A. Zipper, P. Wang, D. Ben-Amotz.
39 "Multivariate Hyperspectral Raman Imaging using Compressive Detection". *Anal.*
40 *Chem.* 2011. 83(13):5086–5092.
41
42
43 [34] D.S. Wilcox, G.T. Buzzard, B.J. Lucier, P. Wang, D. Ben-Amotz. "Photon Level
44 Chemical Classification using Digital Compressive Detection". *Anal. Chim. Acta*
45 2012 755:17–27.
46
47
48
49
50
51
52
53
54
55
56
57
58
59
60

- 1
2
3 [35] J.V. Thompson, J.N. Bixler, B.H. Hokr, G.D. Noojin, M.O. Scully, V.V. Yakovlev.
4 “Single-Shot Chemical Detection and Identification With Compressed Hyperspectral
5 Raman Imaging”. *Opt. Lett.* 2017. 42(11):2169–2172.
6
7
8
9 [36] O.G. Rehrauer, V.C. Dinh, B.R. Mankani, G.T. Buzzard, B.J. Lucier, D. Ben-Amotz.
10 “Binary Complementary Filters for Compressive Raman Spectroscopy”. *Appl.*
11 *Spectrosc.* 2018. 72(1):69–78.
12
13
14
15 [37] C. Scotté, H.B. de Aguiar, D. Marguet, E.M. Green, P. Bouzy, S. Vergnole, C.P.
16 Winlove, N. Stone, H. Rigneault. “Assessment of Compressive Raman Versus
17 Hyperspectral Raman for Microcalcification Chemical Imaging”. *Anal. Chem.* 2018.
18 90(12):7197–7203.
19
20
21
22
23 [38] S. Kosmeier, S. Zolotovskaya, A.C. De Luca, A. Riches, C.S. Herrington, K.
24 Dholakia, M. Mazilu. “Nonredundant Raman Imaging using Optical Eigenmodes”.
25 *Optica* 2014. 1(4):257–263.
26
27
28
29 [39] I. Gusachenko, M. Chen, K. Dholakia. “Raman Imaging Through A Single
30 Multimode Fibre”. *Opt. Express* 2017. 25(12):13782–13798.
31
32
33
34 [40] W. Min, C.W. Freudiger, S. Lu, X.S. Xie. “Coherent Nonlinear Optical Imaging:
35 Beyond Fluorescence Microscopy”. *Annu. Rev. Phys. Chem.* 2011. 62:507–530.
36
37
38
39 [41] N. Dudovich, D. Oron, Y. Silberberg. “Single-Pulse Coherently Controlled
40 Nonlinear Raman Spectroscopy and Microscopy”. *Nature* 2002. 418(6897):512.
41
42
43 [42] D. Oron, N. Dudovich, Y. Silberberg. “Single-Pulse Phase-Contrast Nonlinear
44 Raman Spectroscopy”. *Phys. Rev. Lett.* 2002. 89(27):273001.
45
46
47 [43] H. Frostig, O. Katz, A. Natan, Y. Silberberg. “Single-Pulse Stimulated Raman
48 Scattering Spectroscopy”. *Opt. Lett.* 2011. 36(7):1248–1250.
49
50
51
52 [44] B. von Vacano, T. Backup, M. Motzkus. “Highly Sensitive Single-Beam Heterodyne
53 Coherent Anti-Stokes Raman Scattering”. *Opt. Lett.* 2006. 31(16):2495–2497.
54
55
56
57
58
59
60

- 1
2
3 [45] J. Rehbinder, L. Brückner, A. Wipfler, T. Buckup, M. Motzkus. “Multimodal
4 Nonlinear Optical Microscopy with Shaped 10 fs Pulses”. *Opt. Express* 2014.
5 22(23):28790–28797.
6
7
8
9 [46] H. Frostig, T. Bayer, N. Dudovich, Y.C. Eldar, Y. Silberberg. “Single-Beam
10 Spectrally Controlled Two-Dimensional Raman Spectroscopy”. *Nat. Photonics* 2015.
11 9(5):339.
12
13
14
15 [47] C.W. Freudiger, W. Min, G.R. Holtom, B. Xu, M. Dantus, X.S. Xie. “Highly
16 Specific Label-Free Molecular Imaging with Spectrally Tailored Excitation-
17 Stimulated Raman Scattering (STE-SRS) Microscopy”. *Nat. Photonics* 2011.
18 5(2):103.
19
20
21
22
23 [48] H. Tu, Y. Liu, D. Turchinovich, M. Marjanovic, J.K. Lyngsø, J. Lægsgaard, E.J.
24 Chaney, Y. Zhao, S. You, W.L. Wilson, B. Xu, M. Dantus S.A. Boppart. “Stain-Free
25 Histopathology by Programmable Supercontinuum Pulses”. *Nat. Photonics* 2016.
26 10(8):534.
27
28
29
30
31 [49] M.R. Beversluis, S.J. Stranick. “Enhanced Contrast Coherent Anti-Stokes Raman
32 Scattering Microscopy using Annular Phase Masks”. *Appl. Phys. Lett.* 2008.
33 93(23):231115.
34
35
36
37 [50] A.J. Wright, S.P. Poland, J.M. Girkin, C.W. Freudiger, C.L. Evans, X.S. Xie.
38 “Adaptive Optics for Enhanced Signal in CARS Microscopy”. *Opt. Express* 2007.
39 15(26):18209–18219.
40
41
42
43 [51] E. Da Silva, N.Q. Dao, M.D. Jouan. “New Raman Spectrometer Using a Digital
44 Micromirror Device and a Photomultiplier Tube Detector for Rapid On-Line
45 Industrial Analysis. Part I: Description of the Prototype and Preliminary Results”.
46 *Appl. Spectrosc.* 2008. 62(3):279–284.
47
48
49
50
51
52
53
54
55
56
57
58
59
60

- 1
2
3 [52] E.P. Wagner, B.W. Smith, S. Madden, J.D. Winefordner, M. Mignardi.
4 “Construction and Evaluation of a Visible Spectrometer using Digital Micromirror
5 Spatial Light Modulation”. *Appl. Spectrosc.* 1995. 49(11):1715–1719.
6
7
8
9
10 [53] D. Cebeci, B. Mankani, D. Ben-Amotz. “Recent Trends in Compressive Raman
11 Spectroscopy Using DMD-Based Binary Detection”. *J. Imaging* 2019. 5(1):1.
12
13
14 [54] D.S. Wilcox, G.T. Buzzard, B.J. Lucier, O.G. Rehrauer, P. Wang, D. Ben-Amotz.
15 “Digital Compressive Chemical Quantitation and Hyperspectral Imaging”. *Analyst*
16 2013. 138(17):4982–4990.
17
18
19
20 [55] P. Berto, C. Scotté, F. Galland, H. Rigneault, H.B. De Aguiar. “Programmable
21 Single-Pixel-Based Broadband Stimulated Raman Scattering”. *Opt. Lett.* 2017.
22 42(9):1696–1699.
23
24
25
26 [56] P. Matousek, I.P. Clark, E.R.C. Draper, M.D. Morris, A.E. Goodship, N. Everall,
27 M. Towrie, W.F. Finney, A.W. Parker. “Subsurface Probing in Diffusely Scattering
28 Media using Spatially Offset Raman Spectroscopy”. *Appl. Spectrosc.* 2005.
29 59(4):393–400.
30
31
32
33 [57] P. Matousek. “Inverse Spatially Offset Raman Spectroscopy for Deep Noninvasive
34 Probing of Turbid Media”. *Appl. Spectrosc.* 2006. 60(11):1341–1347.
35
36
37
38 [58] K.M. Khan, S.K. Majumder, P.K. Gupta. “Cone–Shell Raman Spectroscopy (CSRS)
39 for Depth-Sensitive Measurements in Layered Tissue”. *J. Biophotonics* 2015. 8(11-
40 12):889–896.
41
42
43
44
45 [59] Z. Wang, H. Ding, G. Lu, X. Bi. “Use of a Mechanical Iris-Based Fiber Optic Probe
46 for Spatially Offset Raman Spectroscopy”. *Opt. Lett.* 2014. 39(13):3790–3793.
47
48
49
50 [60] Z. Liao, F. Sinjab, G. Gibson, M. Padgett, I. Notingher. “DMD-Based Software-
51 Configurable Spatially-Offset Raman Spectroscopy for Spectral Depth-Profiling of
52 Optically Turbid Samples”. *Opt. Express* 2016. 24(12):12701–12712.
53
54
55
56
57
58
59
60

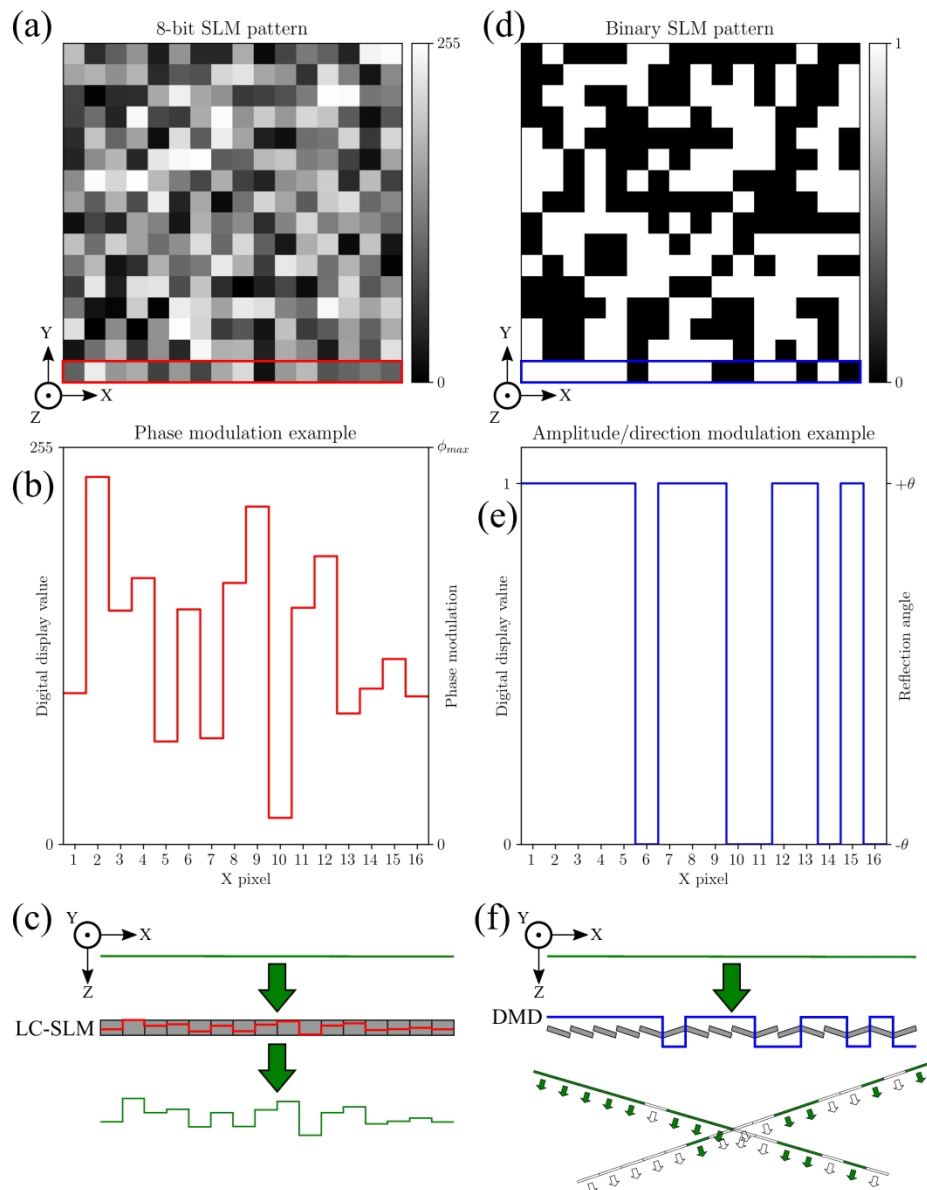
- 1
2
3 [61] Z. Liao, F. Sinjab, A. Nommeots-Nomm, J. Jones, L. Ruiz-Cantu, J. Yang, F. Rose,
4 I. Notingher. "Feasibility of Spatially Offset Raman Spectroscopy for In Vitro and In
5 Vivo Monitoring Mineralization of Bone Tissue Engineering Scaffolds". *Anal.*
6 *Chem.* 2016. 89(1):847–853.
7
8
9
10
11 [62] I. Notingher, A.R. Boccaccini, J. Jones, V. Maquet, L.L. Hench. "Application of
12 Raman Microspectroscopy to the Characterisation of Bioactive Materials". *Mater.*
13 *Charact.* 2002. 49(3):255–260.
14
15
16
17 [63] S. Powell T.S. Leung. "Highly Parallel Monte-Carlo Simulations of the Acousto-
18 Optic Effect in Heterogeneous Turbid Media". *J. Biomed. Opt.* 2012. 17(4):045002.
19
20
21 [64] C.J. Corden, D.W. Shipp, P. Matousek, I. Notingher. "Fast Raman Spectral Mapping
22 of Highly Fluorescing Samples by Time-Gated Spectral Multiplexed Detection".
23 *Opt. Lett.* 2018. 43(23):5733–5736.
24
25
26
27 [65] A.Z. Samuel, S. Yabumoto, K. Kawamura, K. Iwata. "Rapid Microstructure
28 Characterization of Polymer Thin Films with 2D-Array Multifocus Raman
29 Microspectroscopy". *Analyst* 2015. 140(6):1847–1851.
30
31
32
33 [66] K. Kong, C. Kendall, N. Stone, I. Notingher. "Raman Spectroscopy for Medical
34 Diagnostics—From In-Vitro Biofluid Assays to In-Vivo Cancer Detection". *Adv.*
35 *Drug Delivery Rev.* 2015. 89:121–134.
36
37
38
39 [67] K. Kong, C.J. Rowlands, S. Varma, W. Perkins, I.H. Leach, A.A. Koloydenko, H.C.
40 Williams, I. Notingher. "Diagnosis of Tumors During Tissue-Conserving Surgery
41 with Integrated Autofluorescence and Raman Scattering Microscopy". *Proc. Natl.*
42 *Acad. Sci. U. S. A.* 2013. 201311289.
43
44
45
46 [68] S. Takamori, K. Kong, S. Varma, I. Leach, H.C. Williams, I. Notingher.
47 "Optimization of Multimodal Spectral Imaging for Assessment of Resection Margins
48 During Mohs Micrographic Surgery for Basal Cell Carcinoma". *Biomed. Opt.*
49 *Express* 2015. 6(1):98–111.
50
51
52
53
54
55
56
57
58
59
60

- 1
2
3 [69] R. Boitor, K. Kong, D. Shipp, S. Varma, A. Koloydenko, K. Kulkarni, S. Elsheikh,
4 T.B. Schut, P. Caspers, G. Puppels, I. Notingher. “Automated Multimodal Spectral
5 Histopathology for Quantitative Diagnosis of Residual Tumour During Basal Cell
6 Carcinoma Surgery”. *Biomed. Opt. Express* 2017. 8(12):5749–5766.
7
8
9
10
11 [70] K. Kong, F. Zaabar, E. Rakha, I. Ellis, A. Koloydenko, I. Notingher. “Towards Intra-
12 Operative Diagnosis of Tumours During Breast Conserving Surgery by Selective-
13 Sampling Raman Micro-Spectroscopy”. *Phys. Med. Biol.* 2014. 59(20):6141.
14
15
16
17 [71] D.W. Shipp, E.A. Rakha, A.A. Koloydenko, R.D. Macmillan, I.O. Ellis, I.
18 Notingher. “Intra-Operative Spectroscopic Assessment of Surgical Margins During
19 Breast Conserving Surgery”. *Breast Cancer Res.* 2018. 20(1):69.
20
21
22
23 [72] C.J. Rowlands, S. Varma, W. Perkins, I. Leach, H. Williams, I. Notingher. “Rapid
24 Acquisition of Raman Spectral Maps Through Minimal Sampling: Applications in
25 Tissue Imaging”. *J. Biophotonics* 2012. 5(3):220–229.
26
27
28
29 [73] K. Kong, C.J. Rowlands, H. Elsheikha, I. Notingher. “Label-Free Molecular
30 Analysis of Live *Neospora Caninum* Tachyzoites in Host Cells by Selective
31 Scanning Raman Micro-Spectroscopy”. *Analyst* 2012. 137(18):4119–4122.
32
33
34
35 [74] F. Sinjab, D. Awuah, G. Gibson, M. Padgett, A.M. Ghaemmaghami, I. Notingher.
36 “Holographic Optical Trapping Raman Micro-Spectroscopy for Non-Invasive
37 Measurement and Manipulation of Live Cells”. *Opt. Express* 2018. 26(19):25211–
38 25225.
39
40
41
42
43 [75] A.B. Zoladek, R.K. Johal, S. Garcia-Nieto, F. Pascut, K.M. Shakesheff, A.M.
44 Ghaemmaghami, I. Notingher. “Label-Free Molecular Imaging of Immunological
45 Synapses Between Dendritic and T Cells by Raman Micro-Spectroscopy”. *Analyst*
46 2010. 135(12):3205–3212.
47
48
49
50
51
52
53
54
55
56
57
58
59
60

- 1
2
3 [76] F. Sinjab, G. Sicilia, D.W. Shipp, M. Marlow, I. Notinger. "Label-Free Raman
4 Hyperspectral Imaging of Single Cells Cultured on Polymer Substrates". *Appl.*
5 *Spectrosc.* 2017. 71(12):2595–2607.
6
7
8
9 [77] A.A. Adeyemi, N. Barakat, T.E. Darcie. "Applications of Digital Micro-Mirror
10 Devices to Digital Optical Microscope Dynamic Range Enhancement". *Opt. Express*
11 2009. 17(3):1831–1843.
12
13
14 [78] E. Kristensson, J. Bood, M. Alden, E. Nordström, J. Zhu, S. Hultdt, P.-E. Bengtsson,
15 H. Nilsson, E. Berrocal, A. Ehn. "Stray Light Suppression in Spectroscopy Using
16 Periodic Shadowing". *Opt. Express* 2014. 22(7):7711–7721.
17
18 [79] E. Kristensson, A. Ehn, E. Berrocal. "High Dynamic Spectroscopy Using a Digital
19 Micromirror Device and Periodic Shadowing". *Opt. Express* 2017. 25(1):212–222.
20
21 [80] M.G.L. Gustafsson. "Surpassing the Lateral Resolution Limit by a Factor of Two
22 Using Structured Illumination Microscopy". *J. Microsc.* 2000. 198(2):82–87.
23
24 [81] K. Watanabe, A.F. Palonpon, N.I. Smith, A. Kasai, H. Hashimoto, S. Kawata, K.
25 Fujita. "Structured Line Illumination Raman Microscopy". *Nat. Commun.* 2015.
26 6:10095.
27
28 [82] G.M. Gibson, B. Sun, M.P. Edgar, D.B. Phillips, N. Hempler, G.T. Maker, G.P.A.
29 Malcolm, M.J. Padgett. "Real-Time Imaging of Methane Gas Leaks Using A Single-
30 Pixel Camera". *Opt. Express* 2017. 25(4):2998–3005.
31
32 [83] N. Radwell, K.J. Mitchell, G.M. Gibson, M.P. Edgar, R. Bowman, M.J. Padgett.
33 "Single-Pixel Infrared and Visible Microscope". *Optica* 2015. 1(5):285–289.
34
35 [84] K. Fan, J.Y. Suen, W.J. Padilla. "Graphene Metamaterial Spatial Light Modulator for
36 Infrared Single Pixel Imaging". *Opt. Express* 2017. 25(21):25318–25325.
37
38 [85] K. Hashimoto, M. Takahashi, T. Ideguchi, K. Goda. "Broadband Coherent Raman
39 Spectroscopy Running at 24,000 Spectra Per Second". *Sci. Rep.* 2016. 6:21036.
40
41
42
43
44
45
46
47
48
49
50
51
52
53
54
55
56
57
58
59
60

- 1
2
3 [86] M. Tamamitsu, Y. Sakaki, T. Nakamura, G.K. Podagatlapalli, T. Ideguchi, K. Goda.
4
5 “Ultrafast Broadband Fourier-Transform CARS Spectroscopy at 50,000 Spectra/s
6
7 Enabled by a Scanning Fourier-Domain Delay Line”. *Vib. Spectrosc.* 2017. 91:163–
8
9 169.
10
11
12
13
14
15
16
17
18
19
20
21
22
23
24
25
26
27
28
29
30
31
32
33
34
35
36
37
38
39
40
41
42
43
44
45
46
47
48
49
50
51
52
53
54
55
56
57
58
59
60

For Peer Review



Basic concept of phase (a-c) and amplitude (d-f) spatial light modulation. (a) A simulated 8-bit SLM pattern, the bottom row of which is shown in (b), demonstrating the correspondence of image bit value with some phase value. The physical effect of this on a constant phase laser wavefront is shown in (c). A binary modulation pattern is shown in (d), with the data values, which correspond to the direction of a single micro-mirror, shown in (e). For an incident wavefront, this will direct part of the light $+\theta$, and the rest in the $-\theta$ direction.

210x272mm (600 x 600 DPI)

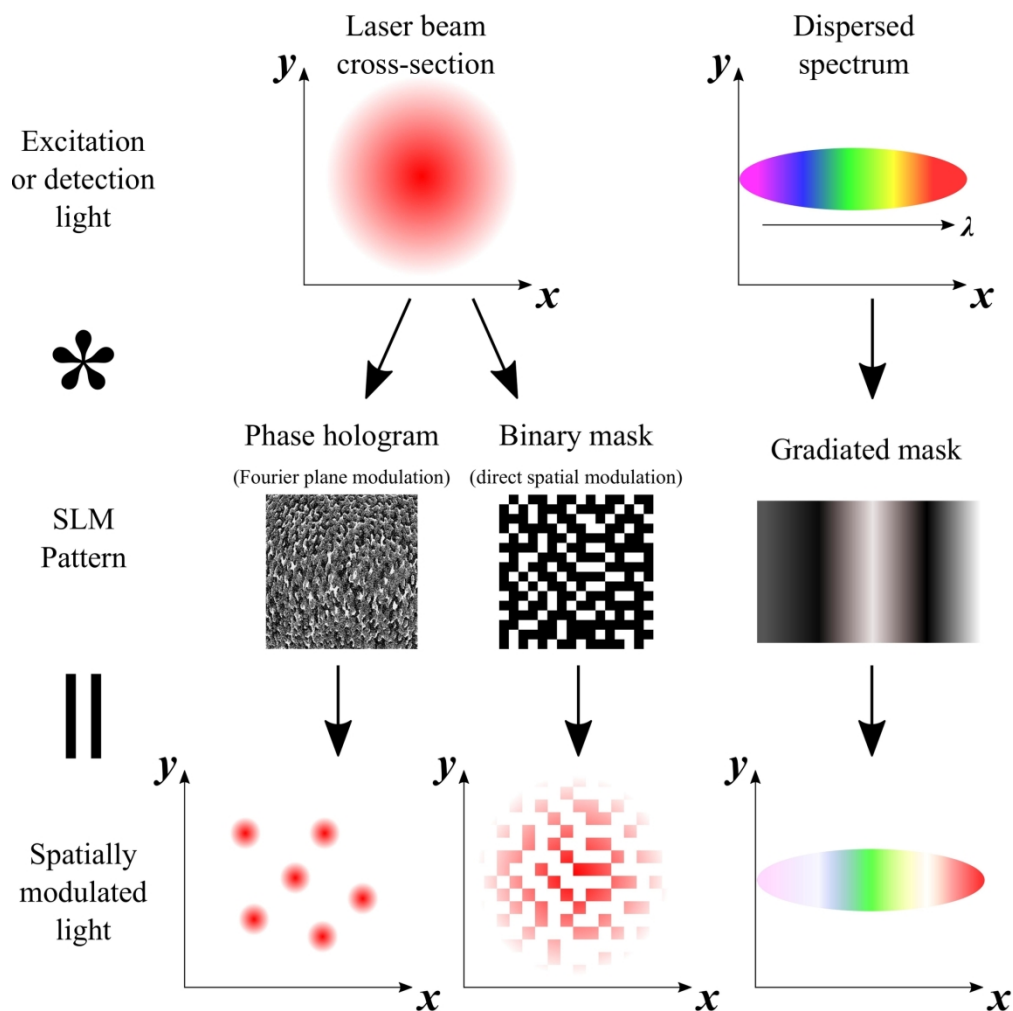
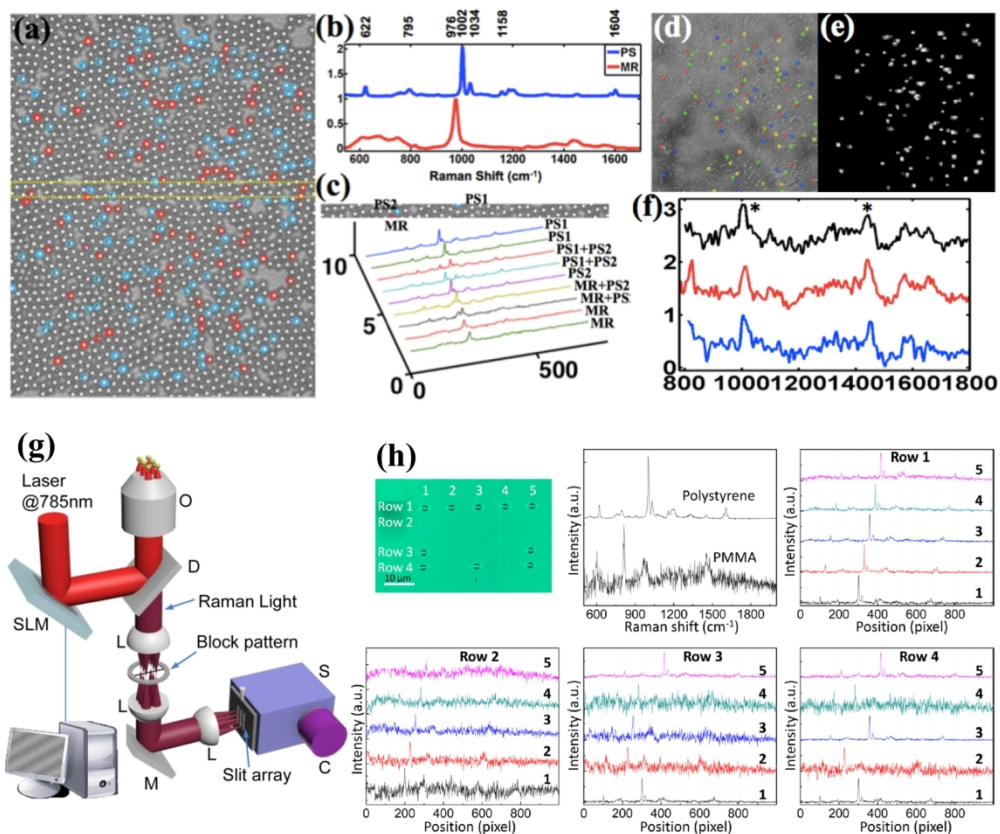


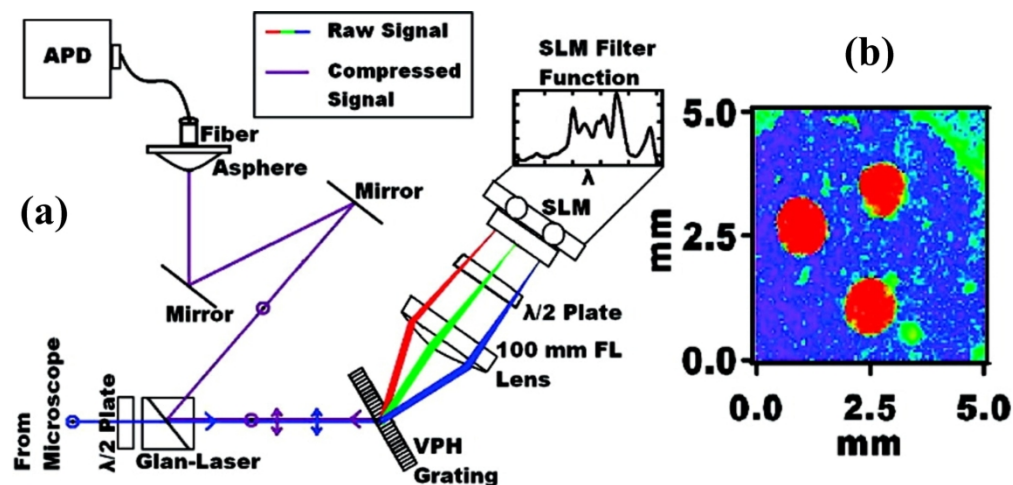
Illustration of types of spatial light modulation relevant to Raman spectroscopy. Common examples include excitation beam cross-sections, spectrally dispersed excitation pulse or spectrally modulated light detection. Patterns can include those corresponding to holographic, spatial, or spectral modulation. Results of these modulations involve multi-point illumination or spatial/spectral modulation. Other types of modulation may be possible. Importance of position of where LC-SLM placed in optical system.

210x210mm (300 x 300 DPI)



Examples of LC-SLMs for multi-point Raman spectroscopy. (a) Qi and Shih[30, 31] initially demonstrated the use of an LC-SLM for programmable multi-point illumination of laser sampling points for fast identification of micro-particles. (b) SLM of an array of trapped particles overlapping in space, using an un-mixing protocol to retrieve overlapped spectra[32].

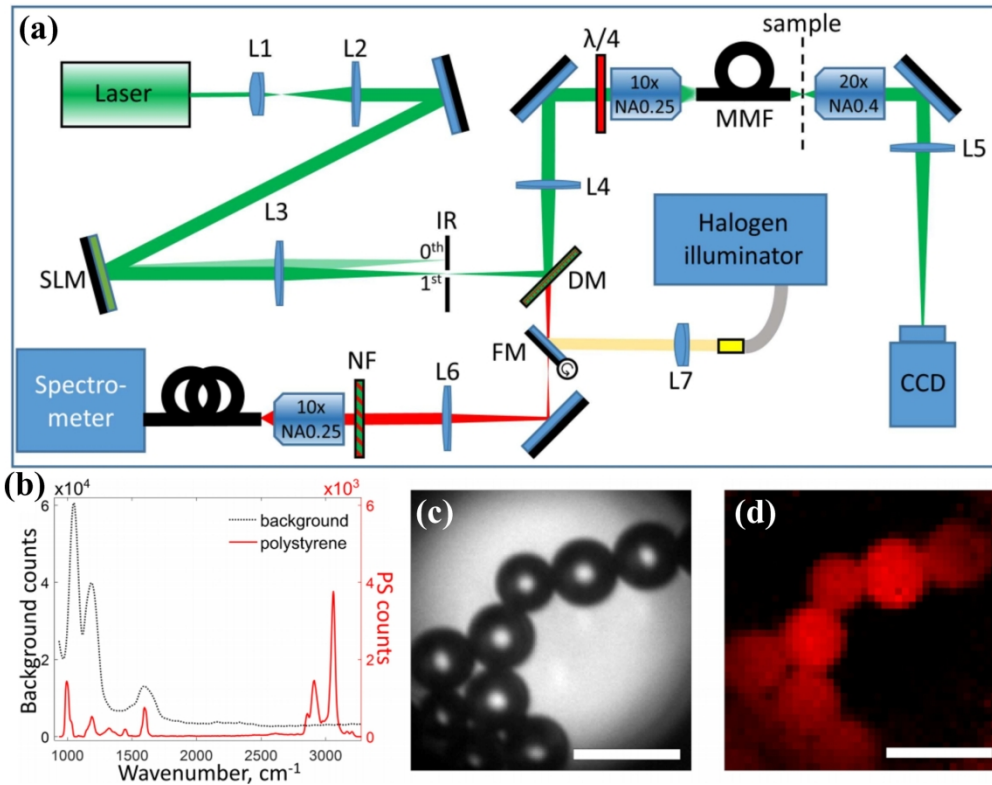
210x174mm (300 x 300 DPI)



(a) Multivariate hyperspectral Raman imaging optical system using LC-LSM. (b) Raman map of aspirin tablet with theophylline embedded (red), 100×100 pixels.

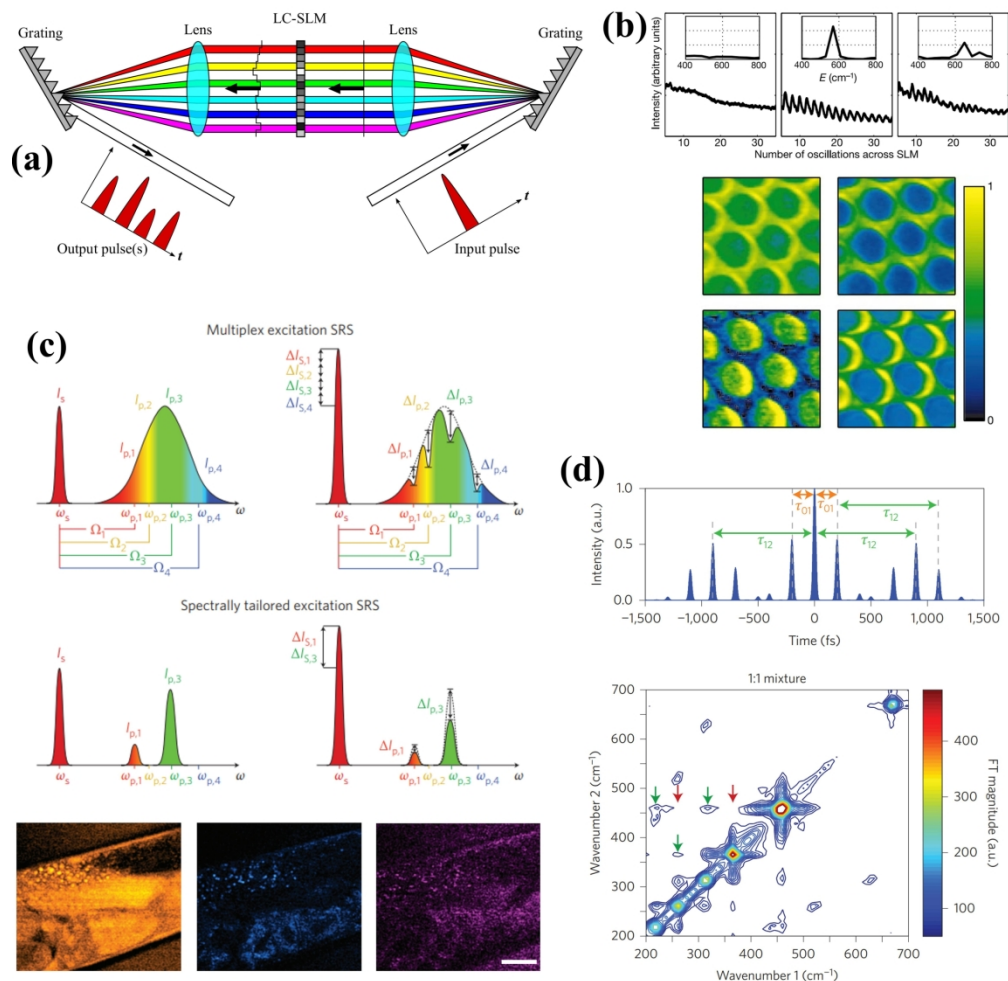
Figure 5. Raman hyperspectral imaging through a multimode fiber. (a) shows the instrument setup. (b) shows example fiber background spectra and polystyrene sample spectra. (c) shows a microscope image and (d) the corresponding point-scanning Raman image of polystyrene beads through the fiber. [38]

210x100mm (300 x 300 DPI)



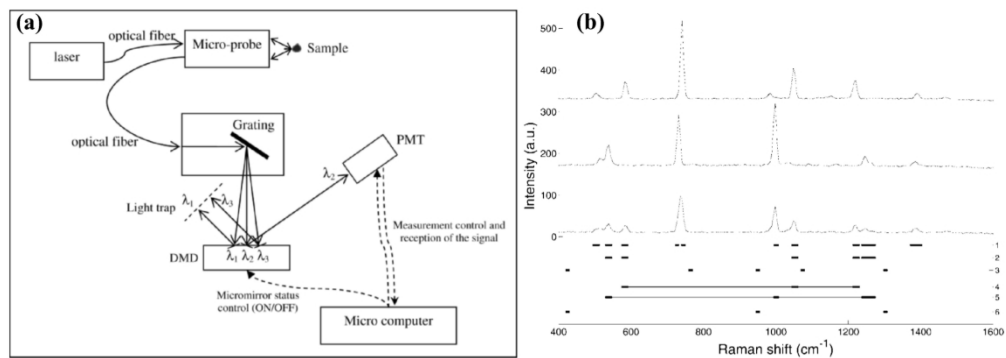
Raman hyperspectral imaging through a multimode fiber. (a) shows the instrument setup. (b) shows example fiber background spectra and polystyrene sample spectra. (c) shows a microscope image and (d) the corresponding point-scanning Raman image of polystyrene beads through the fiber. [38]

207x163mm (300 x 300 DPI)



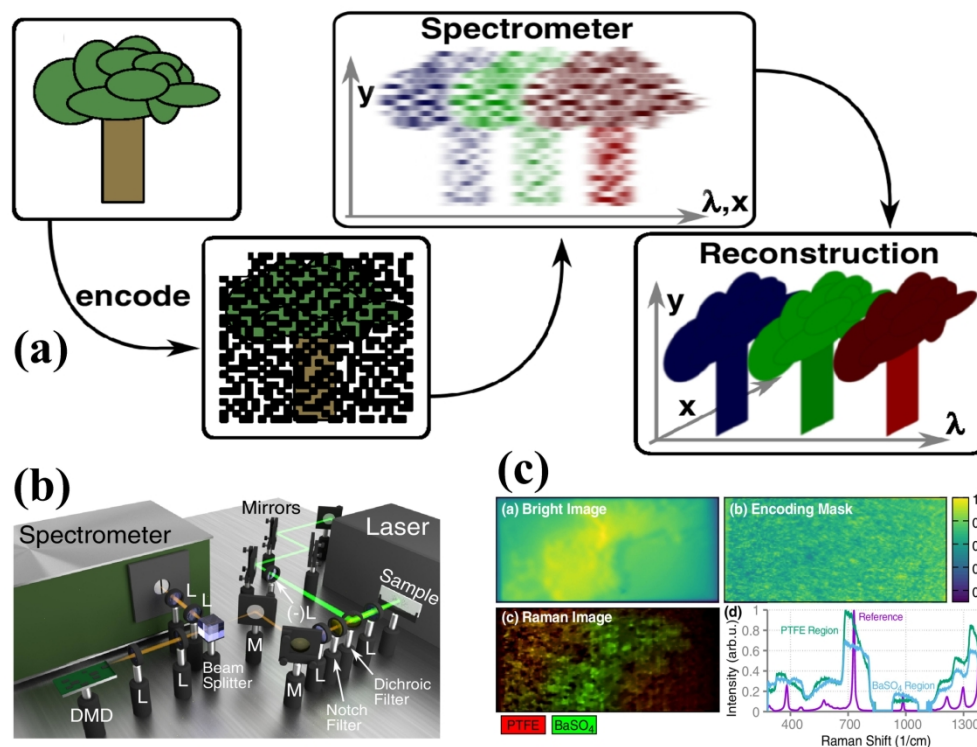
Coherent Raman spectroscopy using LC-SLMs. (a) Schematic of the common 4f pulse shaper used to spectrally modulate femtosecond laser pulses. (b) Single-pulse CARS utilizing an LC-SLM pulse shaper to create a pump and temporally delayed probe. Interferograms with inset spectra of methanol (left), CH₂Br₂ (middle) and (CH₂Cl)₂ (right), and CARS spectroscopic images of CH₂Br₂ in a glass capillary plate [41]. (b) Spectral tailoring of a femtosecond pulse for SRS imaging of multiple vibrational modes. The LC-SLM is used with polarization for amplitude modulation of the spectrum, where the spectral control is desired rather than temporal pulse control. This allowed imaging of proteins (orange, left), oleic acid (blue, center) and stearic acid (magenta, right) within a *C. Elegans* organism [47]. (d) Single-pulse 2D Raman spectroscopy, as an extension of the idea of the single-pulse CARS in (a), where instead two temporally delayed probe pulses are required for the Raman photon echo effect [46].

210x207mm (300 x 300 DPI)



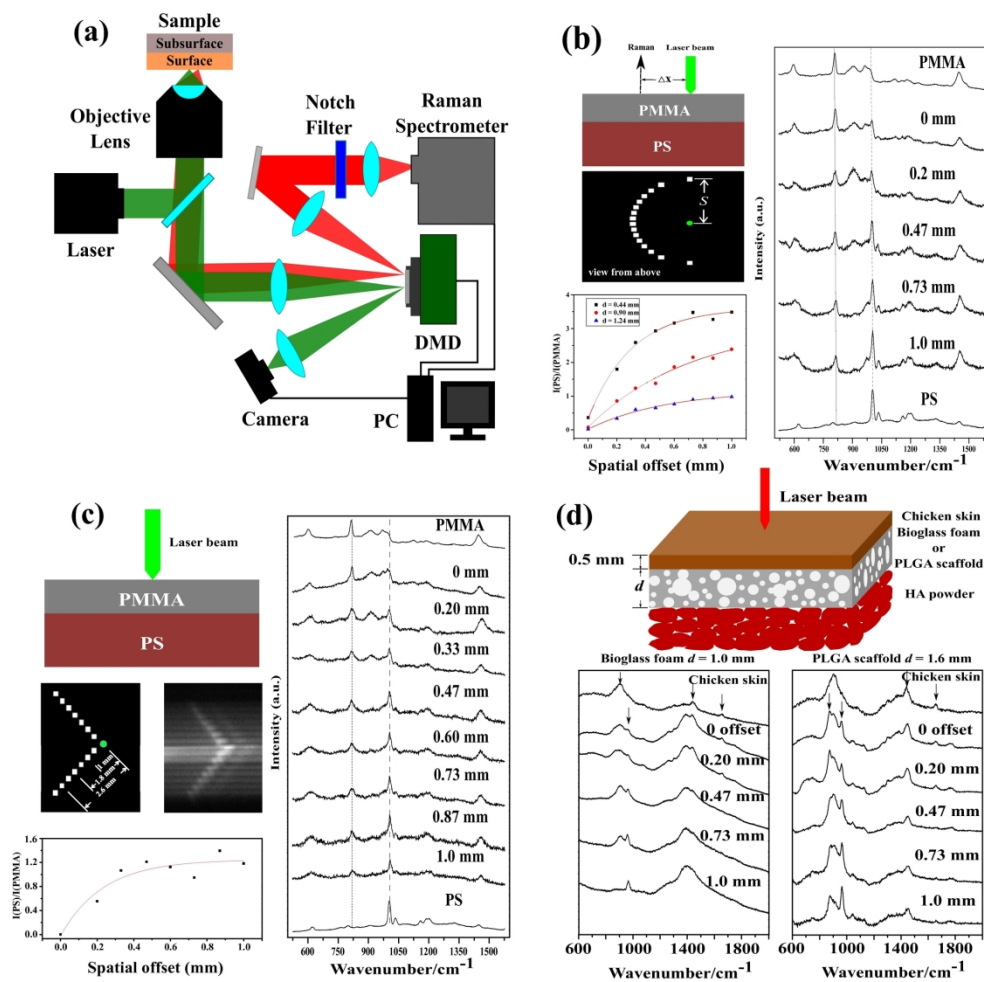
Schematic of a DMD/PMT Raman spectrometer. [51]

209x74mm (300 x 300 DPI)



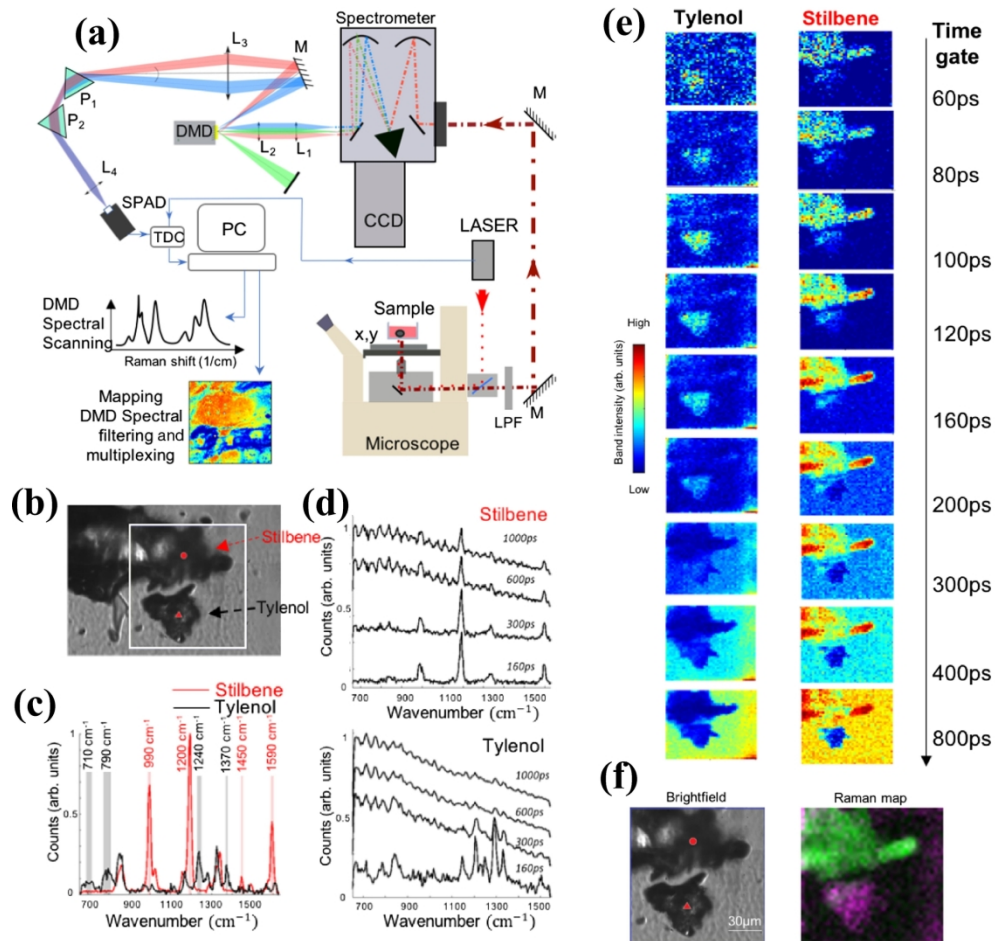
(a) Concept of compressed Raman imaging. The Raman scattered light is firstly encoded with a binary mask on a DMD, then imaged by a spectrometer. The latter spatially shears the image based on the spectral content. Last, a reconstruction algorithm based on the encoding mask recovers hyperspectral images of the original scene. (b) Experimental setup. (c) Recovered Raman image compared to bright-field image.[35]

210x156mm (300 x 300 DPI)



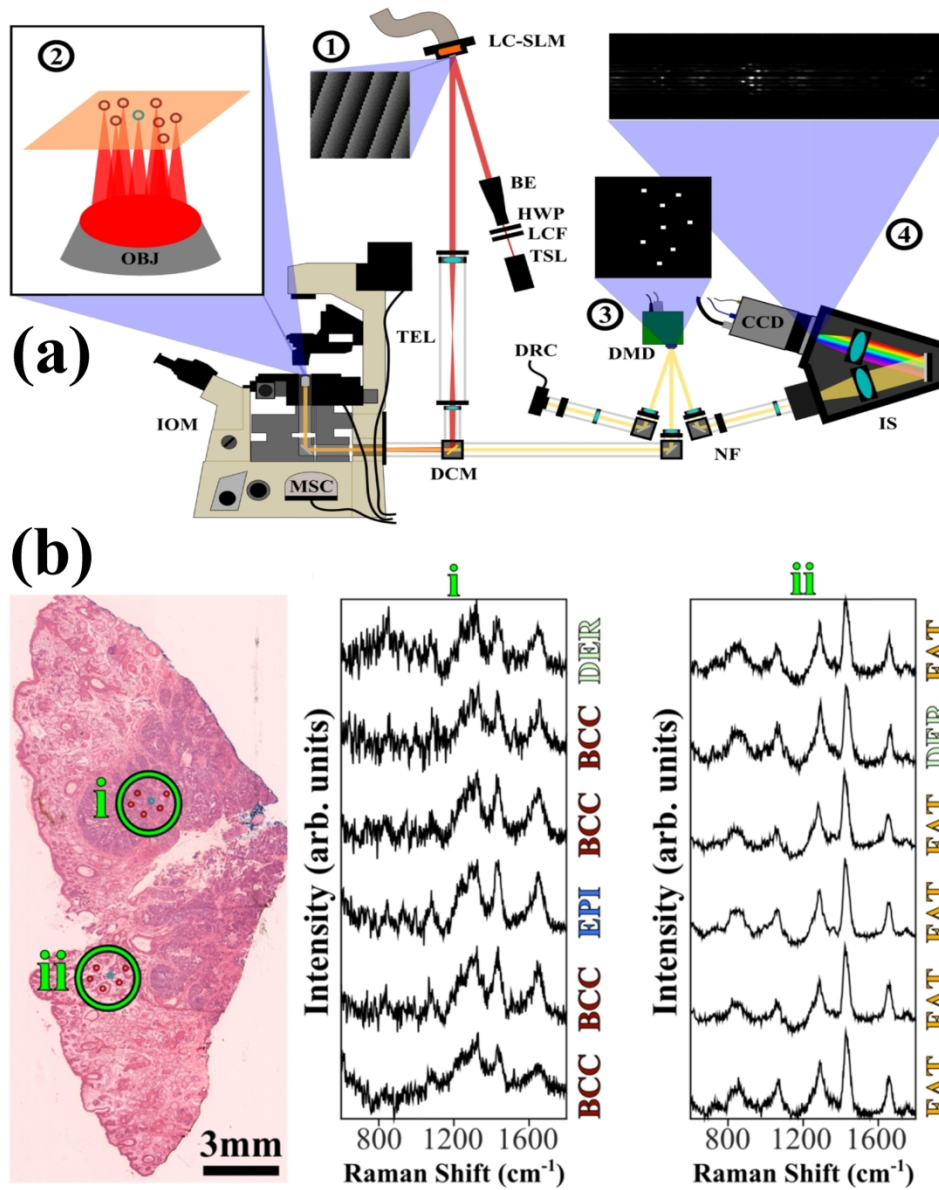
(a) Schematic of SORS optical system using DMD as a computer-controlled spatially offset mask. (b) single-offset semi-annulus collection geometry with high efficiency. (c) multiple-offset collection geometry with low efficiency. [55] (d) DMD-SORS detection of mineralization through chicken skin and tissue engineering scaffolds [60].

209x203mm (300 x 300 DPI)



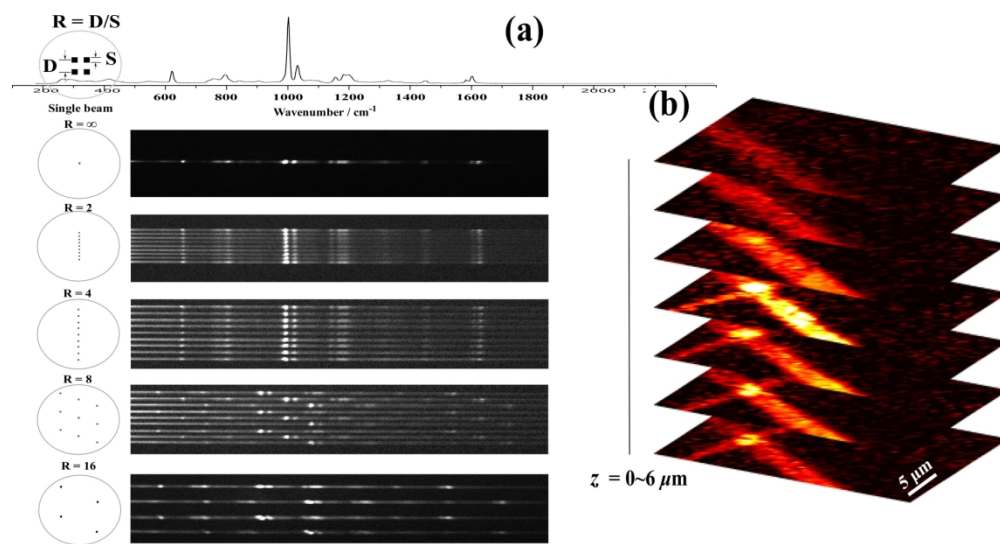
(a) Schematic of DMD/SPAD-based time-gated Raman spectroscopy system. (b) Bright-field image of the Tylenol and stilbene powder on a glass coverslip (mapping area $120\mu\text{m} \times 120\mu\text{m}$). (c) Time-gated spectra of stilbene (circle) and Tylenol (triangle). The bands used for multiplexing are highlighted. (d) Time-gated Raman spectra at the same locations after the addition of the fluorescing dye on top of the sample. (e) Time-gated Raman maps acquired in the DMD multiplexing mode corresponding to the Tylenol (left) and stilbene (right) bands. Acquisition times: 3 minutes for stilbene maps, 27 minutes for the Tylenol maps. (f) Combined pseudo-color Raman map: Tylenol (purple) and stilbene (green); time-gate was 120ps for Tylenol, and 160ps for stilbene, total time: 30 minutes. [64]

210x198mm (300 x 300 DPI)



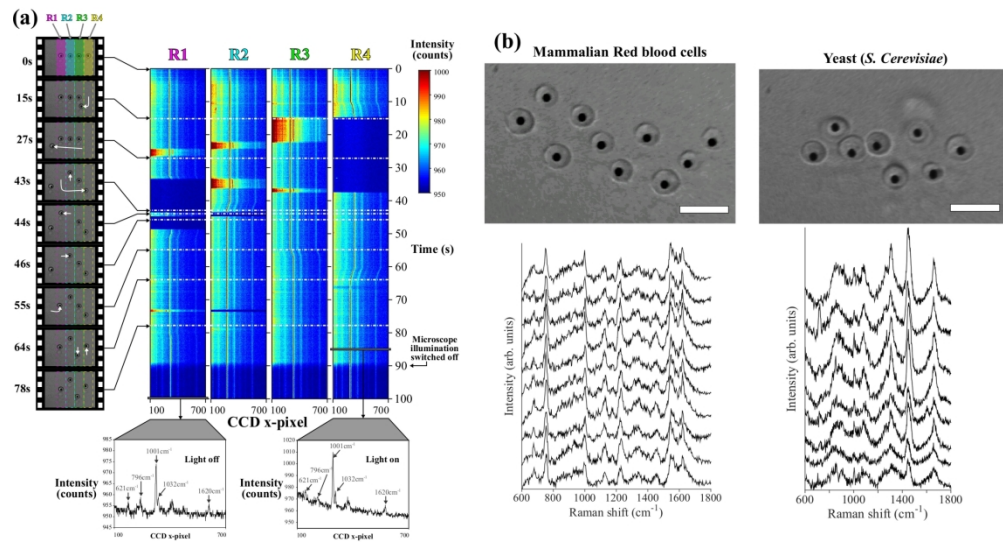
(a) Schematic description of multi-foci Raman system using SLM and DMD. (b) Simultaneous multi-foci Raman measurements on skin tumor resection for cancer diagnosis.[10]

210x262mm (300 x 300 DPI)



SLM/DMD-based multi-foci confocal Raman imaging. (a) SLM/DMD patterns and corresponding Raman CCD images used for multifocal hyperspectral Raman imaging. (b) Optical sectioning by multi-foci Raman imaging of diphenylalanine micro-tubes.[11]

210x111mm (300 x 300 DPI)



Holographic optical trapping Raman micro-spectroscopy. (a) shows video frames and time-course Raman spectra dynamic manipulation-measurement experiment of four trapped 3µm polystyrene beads in four regions of the FOV, from which Raman spectra were acquired at 10Hz (total 40 spectra per second). (b) shows multiple trapped cells in different flexible configurations and controlled excitation power to avoid damage. [74]

210x112mm (300 x 300 DPI)

Applications of Spatial Light Modulators in Raman Spectroscopy

Faris Sinjab^{1,2}, Zhiyu Liao¹, Ioan Notingher^{1*}

¹ School of Physics, University of Nottingham, Nottingham, NG7 2RD, UK

² Current address: Department of Physics, University of Tokyo, Tokyo, 113-0033, Japan

*Email: ioan.notingher@nottingham.ac.uk

Advances in consumer display screen technologies have historically been adapted by researchers across the fields of optics as they can be used as electronically controlled spatial light modulators (SLMs) for a variety of uses. The performance characteristics of such SLM devices based on liquid crystal (LC) and digital-micro-mirror device (DMD) technologies in particular has developed to the point where they are compatible with increasingly sensitive instrumental applications, for example Raman spectroscopy. SLMs provide additional flexibility, from modulation of the laser excitation (including multiple laser foci patterns), manipulation of microscopic samples (optical trapping) or selection of sampling volume (adaptive optics or spatially offset Raman spectroscopy), to modulation in the spectral domain for high-resolution spectral filtering or multiplexed/compressive fast detection. Here, we introduce the benefits of different SLM devices as a part of Raman instrumentation, and provide a variety of recent example applications which have benefited from their incorporation into a Raman system.

Keywords: Raman spectroscopy, spatial light modulators, Instrumentation, Novel methods

Introduction

Raman spectroscopy has continually benefited from a variety of scientific and technological advances. For spontaneous Raman spectroscopy, back-thinned CCD

1
2
3 detectors allowed electronic readout of high-quality spectra at reasonable speeds [1], high-
4 power narrow-linewidth near-infrared lasers provide almost ideal excitation sources for
5 biological samples [2] and high-fidelity optical filters now boast excellent rejection of
6 excitation light with sharp edges close to the excitation frequency[3]. Coupling of these
7 advanced optoelectronic devices to optical or completely different instruments such as
8 scanning probe microscopes has enabled probing the molecular structure of materials with
9 micro- or nanometer scale spatial resolution[4, 5]. All these advances have transformed
10 Raman spectroscopy from an expensive specialist technique to common bench-top
11 instrument used across the physical and life sciences[6, 7, 8]. Of course, advances in
12 technology continue, with new and seemingly far-removed areas of optics finding uses in
13 Raman spectroscopy instrumentation.
14
15

16
17 In this focal point review, we will describe the use of a class of devices termed spatial light
18 modulator (SLM), which are increasingly used in various ways for both spontaneous and
19 nonlinear Raman spectroscopic measurement. Most SLM device technologies were
20 originally developed for use as digital display screen technology, where large arrays of
21 individual electronically addressable pixels must rapidly modulate light by some physical
22 means to produce an image. Perhaps the most familiar example of such a technology is the
23 liquid-crystal display (LCD), where electronic control of the liquid crystal orientation
24 allows control of optical polarization, and, in combination with a polarizer, amplitude
25 modulation of a backlight.
26
27

28 Historically, the prevalence of low-cost consumer LCDs led to their modification and use
29 in optical instruments [9]. Here, instead of the amplitude modulation of an incoherent
30 broad-band backlight used for display purposes, laser light was directed onto the liquid
31 crystal. As laser light is coherent, an ideal spatial cross section of a laser beam will be
32 constant in phase. An LCD screen can modulate the phase by some amount at each pixel
33 at which some proportion of the laser passes through, as illustrated in Figure 1 (a-c). This
34 is the basis for a variety of subsequent techniques, which utilize the spatially-modulated
35 phase of the laser in some way as shown schematically in Figure 2.
36
37

38
39 Figure 1. Basic concept of phase (a-c) and amplitude (d-f) spatial light modulation. (a) A
40 simulated 8-bit SLM pattern, the bottom row of which is shown in (b), demonstrating the
41 correspondence of image bit value with some phase value. The physical effect of this on a
42 constant phase laser wavefront is shown in (c). A binary modulation pattern is shown in
43 (d), with the data values, which correspond to the direction of a single micro-mirror,
44 shown in (e). For an incident wavefront, this will direct part of the light $+\theta$, and the rest
45 in the $-\theta$ direction.
46
47
48

49 One example is for using the spatial-phase modulation to imprint a holographic pattern
50 onto a continuous-wave (CW) laser wavefront. Placing the LCD in the back-focal plane of
51 a lens will result in a Fourier-transform of the spatially varying phase pattern imprinted on
52 the laser at the front focal point. With appropriate choice of phase-hologram, the incident
53 laser can be modulated to focus to multiple spatially separated points, allowing computer-
54 control of multiple laser foci, as used for optical trapping[9] and multi-foci laser scanning
55
56
57
58
59
60

1
2
3 microscopy[10, 11]. LC-SLMs have also commonly been used for shaping ultrafast laser
4 pulses[12] and aberration correction of optical systems[13, 14].
5

6
7 More recent projection display technologies involve completely different approaches to
8 light modulation based on micro-electro-mechanical systems (MEMS). The most
9 successful MEMS display technology is the digital micro-mirror device (DMD) developed
10 by Texas Instruments. These devices utilize arrays of microscopic mirrors (pixel units)
11 whose reflection direction can be individually controlled electronically. Modern digital
12 projectors utilize DMD technology, where video frames are generated by rapidly switching
13 DMD patterns which provides spatial modulation of light amplitude to form the individual
14 colour channel image (different colours of which are generated sequentially).
15

16
17 Amplitude modulation with DMDs has been used for a variety of applications in optics,
18 from single-pixel compressive sensing cameras [15, 16] and spatially-encoded
19 fluorescence spectroscopic imaging [17], to their use as computer-controlled reflective
20 apertures[18]. Many of these optical applications have focused on bright-field and
21 fluorescence microscopy, where DMDs can modify the light fields in some desirable way
22 as shown in Figure 1 (d-f), to improve aspects of measurement such as speed or spatial
23 resolution.
24

25
26 The use of SLMs in other areas of optical sensing preceded their use in Raman
27 spectroscopy, which typically requires high-fidelity optical components to allow efficient
28 excitation and detection, as Raman scattering is a notoriously inefficient process compared
29 to laser-induced fluorescence emission or elastic scattering (typically 5-7 orders of
30 magnitude lower). However, with the improvement of the optical throughput of SLMs,
31 laser excitation and Raman detection losses have approached an acceptable operational
32 range for their usage into Raman spectroscopy instruments.
33

34
35 This review will first describe commonly used SLM devices (primarily LC-SLMs and
36 DMDs), their basic function, and some important parameters to consider for their use.
37 Following this, we will review examples of SLMs used in Raman spectroscopy,
38 highlighting examples where phase-only, amplitude only or phase and amplitude
39 modulation in combination SLMs are utilized. We finish by discussing the outlook for
40 SLMs applied to Raman spectroscopy, and potential new areas for exploration.
41
42
43
44

45 Figure 2. Illustration of types of spatial light modulation relevant to Raman spectroscopy.
46 Common examples include excitation beam cross-sections, spectrally dispersed
47 excitation pulse or spectrally modulated light detection. Patterns can include those
48 corresponding to holographic, spatial, or spectral modulation. Results of these
49 modulations involve multi-point illumination or spatial/spectral modulation. Other types
50 of modulation may be possible. Importance of position of where LC-SLM placed in
51 optical system.
52
53

54 SLM devices

55
56
57
58
59
60

Phase modulation with liquid-crystal spatial light modulators

The LC-SLM is perhaps the most widely utilized SLM device, as liquid crystal technology was one of the earliest digital display screen technologies, the success of which has since led to them becoming relatively low-cost and widespread. Generally, LC-SLMs are phase modulation devices, where controlled phase delay is achieved pixel-by-pixel by electronic control of liquid crystal orientation axis. Nematic liquid crystals are almost exclusively used for 1D or 2D LC-SLMs.

The degree to which a liquid crystal is rotated determines the relative phase-shift of the light at each pixel (note: this implies the impinging light is polarized at a particular angle for efficient modulation). LC-SLMs are usually utilized in reflection mode as the LC control substrate is typically silicon (sometimes specified as liquid crystal on silicon (LCOS)-SLMs) with a high-reflectance layer. Transmission-mode LC-SLMs exist, though are typically lower resolution and have lower optical throughput compared with their reflective counterparts.

LC-SLMs can often modulate broad spectral regions of light, from 400-1600nm, though the total phase shift will vary depending on the exact wavelength. Anti-reflective coatings can be utilized to improve throughput for a particular spectral range. The throughput also depends on other factors than reflection, such as the fill factor (percentage of total display area which can be utilized, related to dead-space between active pixel regions), and the light utilization efficiency (fraction of total incident light which is controllably modulated). Modulation speed is typically in the range of commercial display screen refresh rates (60-120Hz), though with GPU acceleration this can be further increased[19, 20]. **New devices developed by Meadowlark are also capable of faster refresh rates approaching 1 kHz.**

The major manufacturers of LC-SLMs for scientific applications are Hamamatsu, Holoeye and Meadowlark (formerly Boulder Nonlinear Systems). Hamamatsu has a wide selection of LC-SLMs, while Holoeye has the SLM with largest number of pixels, and Meadowlark offer slightly higher-performance optical specifications. Jenoptik have a linear LC-SLM array for femtosecond pulse shaping. Thorlabs and Santec also have some 2D LC-SLM models, with the latter also having a model designed specifically for the UV wavelength region. Cambridge Correlators manufacture a low-cost LC-SLM (~1k GBP) option with relatively lower specifications, though which is still highly suitable for optical trapping[21]. LC-SLM cost is usually linked to optical throughput and pixel number, with the highest resolution and best performing models priced the 20-30k GBP region.

It should be noted that deformable mirror membranes also provide rapid continuous phase modulation which is not polarization-sensitive, though at a much lower resolution than LC-SLMs. Such devices are typically expensive, though are more naturally suited to microscope aberration correction than LC-SLMs[14].

Summary of LC-SLM technology:

Positives:

- High pixel count displays (typically $>1000 \times 1000$, maximum known is 4160×2464 pixels for Holoeye GAEA-2)

- High-resolution phase control, typically ≥ 8 bits for 2π - 8π phase modulation range per pixel
- Some models are available with high fill factor (approaching 100%) and efficient optical throughput with anti-reflection coatings ($>90\%$ reflection).
- Can also be used for amplitude modulation with polarization optics.

Negatives:

- Polarization sensitivity
- High-end models are expensive (order of 20-30k GBP)
- Calculation of optical efficiency is more complex than for purely reflective (mirror-based) devices, as LC modulation involves polarization, reflection and diffraction effects.
- Undesirable higher-order diffraction effects from pixelated nature of device.

Amplitude modulation with digital micro-mirror devices (DMDs)

DMDs have emerged in recent decades from MEMS technology developed by Texas Instruments primarily for projector display purposes. Image contrast in such an application is controlled by rapidly switching micro-mirror tilt angle with variable duty cycle corresponding to grayscale control for each colour channel, with cycling through colour channels building up a time-averaged colour image. This technology has been exploited for binary and grayscale amplitude modulation in various areas of microscopy and imaging. Fill factors are typically high, and as the technology is mirror-based, total throughput can be above 90% for visible-NIR light. Thus applications for modulating weak Raman photons can be implemented with negligible degradation of the signal.

Texas instruments are the major manufacturer of DMD display devices. A low-cost DMD option is to modify a commercial projector product or evaluation board, such as the popular DLP Lightcrafter. Higher cost research-specific models also exist with direct access to the DMD display surface, with high-speed capability such as the Vialux V-700 with $>20\text{kHz}$ 1-bit array frame switching rates possible. Other than Texas Instruments, the Fraunhofer Institute for Photonic Microsystems also produce R&D MEMS mirror devices, including one-dimensional DMDs with up to 1 MHz frame rate.

Summary of DMD technology:

Positives:

- Widespread commercial availability resulting in low-cost options e.g. DLP Lightcrafter Evaluation development board available for approximately 500 GBP (requires some modification to access DMD display).
- Rapid refresh rates (typically several hundred Hz minimum) possible when using pre-determined low bit-depth patterns stored in on-device flash memory.
- Alternative display cable interfacing is simple to implement and allows standard video rate (60-120Hz) of arbitrary patterns generated in real-time
- Optical losses are minimal in the UV-VIS-NIR, as the technology is based on aluminium mirrors.
- High-resolution displays are available (up to 3840×2160 in current DLP660TE devices)

- Not polarization-sensitive

Negatives:

- Only amplitude modulation based on tilt-angle is possible
- Shallow mirror angles can make alignment difficult and often increases instrument size due to extra optics required. This is solved using integrated optics in commercial projector boards, which may not always be possible for prototyping in a lab on an optical table
- Pixelated spatial profile can generate unwanted higher-order diffraction effects
- Primarily designed for use in visible spectral region, though NIR-optimized models are emerging.

Examples of SLMs used in Raman spectroscopy

Uses of phase-modulation SLMs

Phase modulation SLMs are typically utilized in the excitation stage of a Raman instrument to modify the laser beam in various ways. While it may be possible to utilize modern LC-SLMs for modulating the detected Raman scattering, optical throughput is typically lower compared with mirror-based SLM devices, and laser photons are generally more readily available than Raman photons. Additionally, the effects of phase control on coherent monochromatic laser light offers additional effects which can be capitalized upon, such as holographic phase patterning for multiplexed beam steering. Here, we will discuss the various applications of LC-SLMs demonstrated in Raman spectroscopy instruments for enhanced control of the excitation laser source in some way.

Spatially controlled spontaneous Raman excitation

One of the biggest drawbacks in spontaneous Raman spectroscopy is the long acquisition times required for measurement, due to the inherently low Raman scattering cross-section for most materials of interest. The spontaneous Raman scattering intensity can be written as $I = \sigma NFD$ where σ is the Raman scattering cross section, N is the number of scatterers in the measurement volume, F is the source excitation flux, and D is the detection efficiency. Of these terms, F is the only parameter that can be readily adjusted in an experiment by increasing the laser power. However, this soon reaches a limit imposed either by available laser technology, or by sample damage threshold (particularly for life science applications). Thus, in order to further improve measurement times, smarter approaches to sampling must be considered.

Several strategies have been proposed for increasing the speed of Raman hyperspectral imaging, including multi-foci excitation, line-scanning and wide-field Raman imaging [10, 22, 23, 24]. One of the most direct approaches to such sampling is simply to create multiple parallelized laser excitation points for readout. Many approaches to this have been demonstrated, from using fixed optical elements such as lens arrays [25, 22, 26], to scanning galvo mirrors [27, 28, 29], and LC-SLMs [30, 31, 32]. The LC-SLM approach allows the most flexibility, and truly simultaneous excitation (opposed to temporal scanning of a single high-power beam), though also involves added computational

1
2
3 complexity and higher cost. Additionally, LC-SLMs generating multiple laser foci can also
4 be utilized for holographic optical trapping (HOT). The first use of LC-SLMs for optical
5 trapping in Raman spectroscopy was demonstrated by Qi and Shih, who were able to
6 measure polymer microparticles at 1,000 sampling points per second semi-randomly from
7 a $100 \times 100 \mu\text{m}^2$ field of view. Measurement of bacterial spores was also demonstrated at
8 a measurement rate of 2.5 sampling points per second. In this study, patterns were
9 generated such that sampling points did not overlap along one axis, as this would create
10 cross-talk on the CCD used for Raman spectroscopic measurement.
11
12

13
14 For measurements involving sampling points overlapping on one axis, cross-talk can be
15 avoided in several ways. Kong et al, demonstrated galvo mirrors for re-alignment through
16 a Raman CCD slit, however this time-shared scheme would result in a loss of efficiency if
17 an LC-SLM were used for power-shared excitation. In order to use completely power-
18 shared LC-SLM excitation efficiently, the group of Chan developed an electronically
19 controlled 4×5 block pattern matched to a slit array for Raman measurement from a multi-
20 focal array grid pattern. With knowledge of which slit patterns were used for measurement,
21 overlapping spectra could be computationally unmixed in post processing, which was
22 demonstrated for trapped arrays of polystyrene and PMMA microbeads.
23
24
25

26
27 **Figure 3. Examples of LC-SLMs for multi-point Raman spectroscopy. (a) Qi and**
28 **Shih[30, 31] initially demonstrated the use of an LC-SLM for programmable multi-point**
29 **illumination of laser sampling points for fast identification of micro-particles. (b) SLM of**
30 **an array of trapped particles overlapping in space, using an un-mixing protocol to retrieve**
31 **overlapped spectra[32].**
32
33

34
35 Multivariate hyperspectral imaging (MHI) based on compressive detection is an alternative
36 to achieve fast Raman mapping without using high laser power. MHI is a compressive
37 sampling strategy that utilizes a low-noise channel detector to simultaneously collect all
38 the photons transmitted by a multivariate optical filter. In cases when the CCD read-out
39 noise is the limiting factor, single channel detectors will have lower noise, and the
40 collection can be much faster than CCD-based spectral detection methods. The multivariate
41 filter plays a vital role in the MHI detection strategy, as it selects the photons to be collected,
42 and Raman spectra are later reconstructed based on the spectral shape using the
43 sequentially measured Raman photons. For detection of chemical mixtures, multiple
44 spectral patterns may be needed for classifying the binned photons. Thus the optical filter
45 should be rapidly switched to implement different spectral patterns. Spatial light
46 modulators are ideal for such an application, as they can be programmed to produce
47 variable filters with different spectral shapes with a rapid refresh rate ensuring fast
48 transitions between filter patterns. A compressed detection of Raman spectroscopy was
49 also realized using two types of SLM: LC-SLM [33] and DMD[34, 35, 36, 37]. Here we
50 will briefly introduce the LC-SLM based system, as the DMD-based system will be
51 presented in the amplitude-modulation SLM section of this review. Figure 4(a) shows the
52 diagram of the LC-SLM based compressive detection optics. A LC-SLM was placed at the
53 plane where a CCD camera located in a conventional Raman spectrometer. Raman
54 scattered light was dispersed by a volume holographic grating and directed on the SLM.
55
56
57
58
59
60

1
2
3 The SLM filter functions modulated the signal based on the polarization and reflected the
4 desired photons back into the detection path. The reflected signal was then collected by a
5 single channel detector, such as an avalanche photodiode (APD). Chemical imaging of an
6 aspirin and theophylline composite sample demonstrates the high-throughput of
7 multivariate hyperspectral Raman spectroscopy using compressive detection. The total
8 acquisition time of the chemical map shown in Figure 4(b) was 30 s (100×100 pixels).

9
10 A similar approach to spatially-encoded imaging was demonstrated by the group of K.
11 Dholakia, who used an LC-SLM to create spatial eigenmodes for effective wide-field
12 Raman imaging [38]. This approach used orthogonal 2D laser excitation patterns created
13 by an LC-SLM to excite Raman scattering and measured using a standard Raman
14 spectrometer. For sequential Raman measurements with different eigenmode patterns,
15 Raman hyperspectral images could be generated, with adjustable SNR and spatial
16 resolution depending on the number of sequential patterns utilized. Raman hyperspectral
17 imaging of polymers, pharmaceuticals and SERS probes was demonstrated with this
18 approach.
19

20 The same group also utilized the first-order diffracted light from an LC-SLM for Raman
21 measurement through a single multimode optical fiber [39]. The SLM allowed the
22 diffraction-limited excitation laser point to be spatially controlled in 3D at the distal end of
23 the fiber, as shown in Figure 5(a). This enabled point-scanned imaging, which was
24 demonstrated for polystyrene beads (Figure 5(b-d)), bacteria clusters, and pharmaceuticals.
25 This approach holds promise for endoscopic Raman hyperspectral imaging in biomedical
26 applications.
27
28
29
30

31 Figure 4. (a) Multivariate hyperspectral Raman imaging optical system using LC-LSM.
32 (b) Raman map of aspirin tablet with theophylline embedded (red), 100×100 pixels.
33
34
35

36 Figure 5. Raman hyperspectral imaging through a multimode fiber. (a) shows the
37 instrument setup. (b) shows example fiber background spectra and polystyrene sample
38 spectra. (c) shows a microscope image and (d) the corresponding point-scanning Raman
39 image of polystyrene beads through the fiber. [38]
40
41
42

43 Pulsed laser modulation in coherent Raman spectroscopy

44 Coherent Raman spectroscopy (CRS) techniques, in which pico- or femto-second pulsed
45 laser excitation is used to excite molecular vibrations via the third-order nonlinear
46 susceptibility, also have examples where SLMs have been utilized to improve the
47 instrument in some way. However, whereas LC-SLMs used in spontaneous Raman
48 spectroscopy are typically inspired by fluorescence or optical trapping, applications in CRS
49 typically borrow from other multiphoton microscopy or ultrafast pulse shaping techniques.
50 The two dominant CRS techniques are coherent anti-Stokes Raman (CARS) and stimulated
51 Raman scattering (SRS), both of which provide orders of magnitude speed up in
52 measurement acquisition times, though typically at the expense of spectral resolution and
53 increased complexity. Both techniques typically require multiple laser wavelengths to
54 generate a coherent vibrational state, and to probe this state[40].
55
56
57
58
59
60

1
2
3
4 The first demonstration of coherent Raman spectroscopy with spatial light modulators was
5 by group of Silberberg, who used an LC-SLM for pulse shaping[41]. While the refresh rate
6 of any SLM (or indeed most optical devices) is completely out of reach of ultrashort pulse
7 timescales, ruling out direct temporal modulation, spatial modulation of the dispersed pulse
8 spectrum can instead be used for pulse shaping. For a femtosecond pulse, modulation of
9 the pulse spectrum will result in the temporal profile of the pulse being modified (as the
10 two are linked via Fourier transformation). This is typically implemented as a $4f$ pulse
11 shaper, shown in Figure 6 (a), where the SLM is placed at the central position of a unity
12 magnification telescope with diffraction gratings at the front and back focal planes of the
13 telescope[12].
14
15

16
17 Femtosecond pulses are used for time-domain CARS, which is based on impulsive
18 stimulated Raman scattering, whereby all modes within the pulse bandwidth are excited by
19 a pump pulse, and CARS detection carried out using a time-varying probe pulse, generating
20 a CARS interferogram, which upon Fourier transformation produces a CARS spectrum.
21 The group of Silberberg et al utilized a pulse shaper to convert a single pulse into a pump
22 pulse and temporally varying probe pulse, simplifying the optical setup considerably. This
23 was possible using an LC-SLM in a pulse-shaping layout, to convert a single pulse into
24 two controllably temporally separated pulses, which were utilized as pump and probe for
25 the CARS process[41]. Using this approach, CARS spectra were able to be acquired in the
26 $400\text{-}800\text{cm}^{-1}$ spectral range, and CARS images of CH_2Br_2 liquid in a glass capillary plate
27 were demonstrated (Figure 6 (b)). Using the core idea of single-beam pulse shaping, many
28 other Raman-based excitation schemes have also been demonstrated including phase-
29 contrast[42] and single-beam SRS[43]. The group of M. Motzkus have also extended the
30 single-beam CARS approach by utilizing the attenuated edge of a pulse spectrum in the
31 LC-SLM pulse-shaper as a local oscillator for heterodyne amplification to increase
32 sensitivity by several orders of magnitude[44], and have also combined the pulse-shaping
33 CARS technique with other multiphoton imaging modalities[45]. Single-pulse two-
34 dimensional Raman spectroscopy was also demonstrated as shown in Figure 6 (d), where
35 pulses at three different excitation time-points were generated[46]. These methods utilize
36 the impulsive stimulated Raman process driven by short (femtosecond) but broadband laser
37 pulses to excite all vibrational modes within the pulse bandwidth. However, many CARS
38 and SRS instruments utilize two or more narrowband picosecond pulses to excite Raman
39 scattering from specific targeted vibrational modes. Halfway between is the use of both
40 femtosecond and picosecond pulses for multiplex SRS/CARS. Freudiger et al utilized an
41 SLM to tailor the femtosecond pulse spectrum in a multiplex SRS microscope, allowing
42 selective SRS excitations of vibrational modes within the pulse bandwidth as shown in
43 Figure 6 (c) [47]. A pulse shaping configuration was also used for programmable control
44 of a supercontinuum source, allowing shorter (femtosecond) pulse excitation for optimized
45 second/third harmonic generation and two-/three- photon fluorescence microscopy, while
46 picosecond pulses were programmed for CARS and SRS excitation[48]. Stranick et al. also
47 used LC-SLMs for phase-contrast CARS microscopy, where the SLM in order to create a
48 digital phase mask[49].
49
50

51 Phase-modulation with a deformable mirror membrane was demonstrated by Wright et al.
52 for adaptive aberration correction of a picosecond pulsed laser for deep-tissue CARS
53
54
55
56
57
58
59
60

1
2
3 microscopy[50]. In principle, LC-SLMs can be utilized for such aberration correction,
4 though deformable mirrors are better suited to this specific task as their phase modulation
5 is continuous, not pixelated [14].
6
7
8

9
10 Figure 6. Coherent Raman spectroscopy using LC-SLMs. (a) Schematic of the common
11 $4f$ pulse shaper used to spectrally modulate femtosecond laser pulses. (b) Single-pulse
12 CARS utilizing an LC-SLM pulse shaper to create a pump and temporally delayed probe.
13 Interferograms with inset spectra of methanol (left), CH_2Br_2 (middle) and $(\text{CH}_2\text{Cl})_2$
14 (right), and CARS spectroscopic images of CH_2Br_2 in a glass capillary plate [41]. (b)
15 Spectral tailoring of a femtosecond pulse for SRS imaging of multiple vibrational modes.
16 The LC-SLM is used with polarization for amplitude modulation of the spectrum, where
17 the spectral control is desired rather than temporal pulse control. This allowed imaging of
18 proteins (orange, left), oleic acid (blue, center) and stearic acid (magenta, right) within a
19 *C. Elegans* organism[47]. (d) Single-pulse 2D Raman spectroscopy, as an extension of
20 the idea of the single-pulse CARS in (a), where instead two temporally delayed probe
21 pulses are required for the Raman photon echo effect[46].
22
23
24
25

26 Uses of amplitude modulation SLMs

27 Raman spectrometer using a DMD and single-element detectors
28
29
30

31 Figure 7. Schematic of a DMD/PMT Raman spectrometer. [51]

32 Wagner *et al* first proposed a relatively inexpensive solution to build an optical
33 spectrometer using a digital micromirror device (DMD) and a single-element detector, such
34 as a photomultiplier tube (PMT) [52]. Quyen *et al* subsequently demonstrated the use of a
35 DMD/PMT spectrometer in Raman applications (schematic description shown in Figure
36 7(a)) [51]. Compared to typical Raman spectroscopy instruments, the major change in this
37 prototype is the use of a DMD as light modulator in the detection path to select Raman
38 light with specific wavelengths to the PMT. The dispersed Raman light from the grating
39 is directed onto the DMD, which consists of 1024×768 micro-mirrors that can be tilted \pm
40 12° relative to the normal of the display surface. The 1024 columns of micro-mirrors are
41 divided into 256 groups. By sequentially directing a group of mirrors towards the PMT
42 (with other mirrors directed in the opposing direction), a Raman spectrum can be obtained,
43 in a similar manner as with a Raman spectrometer based on a scanning monochromator.
44 To maintain good spectral resolution for the measured spectrum, only a few columns of
45 micromirrors are switched on at a time, though this leads to lengthy measurement time
46 when acquiring a full spectrum. It was later suggested that analytical precision could be
47 maintained if multiple characteristic peaks of a sample spectrum are measured at the same
48 time, which can be facilitated by the DMD/PMT configuration for multi-peak Raman
49 measurement. By taking the advantage of DMD/PMT Raman spectrometer, Quyen *et al*
50 demonstrated that wavelength selection sampling is almost as good as whole spectrum
51 recording in terms of qualitative analysis and quantitative analysis. Identification and
52 quantification of binary and ternary mixtures of chemicals were accurately achieved by
53
54
55
56
57
58
59
60

selective multi-peak sampling (see Figure 7(b)). Compared to whole spectrum analysis, the total measurement was significantly shortened by skipping the recording of non-informative data in the spectrum. However, *a priori* knowledge of the sample spectrum is required for peak selection.

The acquisition speed can be further improved by combining DMD/PMT Raman spectrometer with compressive detection approaches, **which has been reviewed recently [53]**. The use of DMD to encode a Raman spectrum for measurement onto a single-pixel detector was achieved by Ben-Amotz *et al* using binary filters, enabling rapid chemical classification and simultaneous imaging of two chemical species in a sample. [34, 54] Since the switching time of DMD mirrors can be as short as **10 μ s**, multiple filters can be quickly configured with varying integration times to achieve rapid Raman measurements. Rather than sequentially select Raman bands on the DMD, rapid chemical classification was implemented by differentiating the Raman scattering photons based on the filter configuration and integration time for each filter set. The filters were generated based on the pure Raman spectral features of the components of interest. In other words, training spectra of the chemicals to be identified are required to construct accurate filters for compressive detection. Similar to the DMD/PMT-based Raman spectrometer, full Raman spectra of the samples were measured by DMD-based wavelength scanning. The obtained training spectra were then used as an input to generate optimal filters. There are different ways to generate filters. Digital and analogue compressive detection strategies have been used for constructing filters. As DMD works only in a binary manner, digital filters are more suitable. In contrast, LC-SLM works better with analogue detection strategy [33].

Later, the same group extended the DMD-based binary compressive detection strategy by using two detectors to collect the Raman photons in two different channels [36]. With two detectors, all Raman photons can be collected by using a pair of complementary binary filters that direct photons toward either of the detectors. The optical layout is slightly different from that which uses a single detector, as the two detectors are facing the $\pm 12^\circ$ position relative to the DMD, respectively. By using complementary binary filters, the number of measurements can be reduced compared to single detector strategy. Moreover, the most significant advantage of using two detectors is that when only two significant components to be classified or quantified, only a single pair of complementary filters is needed, and there is no dead-time or delay due to switching the DMD mirrors. For classifying an acetone and benzene liquid mixture, the total measurement time was 10% of the single detector approach. Raman imaging of a two-component sample mixture with $600 \times 600 \mu\text{m}$ area (240×240 pixels) was finished in 4 s, demonstrating the capability of DMD/PMT-based compressive detection for fast hyperspectral Raman imaging.

More recently, Scotte *et al* compared the speed performance of DMD/PMT-based compressive Raman imaging to two state-of-the-art hyperspectral Raman imaging systems [37]. The configuration of the DMD/PMT-based system was similar to the one shown in Figure 7(a), while the other two instruments using a CCD or an EMCCD. By imaging powder mixture samples mimicking micro-calcifications relevant for breast cancer diagnosis, the authors showed that the DMD/PMT-based compressive system allows $100\times$ and $10\times$ faster acquisition speed than the CCD- and EMCCD-based systems, respectively.

1
2
3
4
5
6 Figure 8. (a) Concept of compressed Raman imaging. The Raman scattered light is firstly
7 encoded with a binary mask on a DMD, then imaged by a spectrometer. The latter
8 spatially shears the image based on the spectral content. Last, a reconstruction algorithm
9 based on the encoding mask recovers hyperspectral images of the original scene. (b)
10 Experimental setup. (c) Recovered Raman image compared to bright-field image.[35]
11

12 While DMD/PMT-based compressive detection provides a means to increase the speed for
13 chemical classification and imaging, the original spectral information is lost during the
14 computational analysis, as the latter is performed before data acquisition. Thompson *et al*
15 [35] reported a technique of single-shot compressed hyperspectral Raman imaging by
16 utilizing a combination of DMD and spectrometer to achieve spatio-spectral compressive
17 detection, where full spectral information can be retrieved after reconstruction. Instead of
18 a single-channel detector, a spectrometer consisting of a grating and a CCD camera was
19 used for detection. Figure 8(a) shows the concept of this approach to compressed Raman
20 imaging. Similar to DMD/PMT-based compressive detection, here the DMD was used to
21 encode a binary mask onto the image of the sample. The grating in the spectrometer then
22 sheared the spectral information in the spatial domain, and the CCD detector captured the
23 full spectral information at each pixel of the acquired image. Afterwards, a full-resolution
24 hyperspectral data cube was recovered from the encoded two-dimensional CCD image.
25 Hyperspectral Raman image of barium sulfate (BaSO_4) powder on an
26 olytetrafluoroethylene (PTFE) block was successfully recovered from a compressed data.
27 The latter was obtained in a single acquisition with CCD integration time of 5 s. Compared
28 to the aforementioned DMD/PMT-based compressive detection strategy, speed may not be
29 an advantage for DMD/CCD-based compressed sensing, but the key advantage lies in the
30 fact that full spectral information is reserved, and no prior knowledge of the sample is
31 needed for constructing the encoding mask.
32
33
34
35

36 All examples of DMD-based sensing above utilized spontaneous Raman spectroscopy,
37 however broadband SRS measurements have also been demonstrated recently utilizing a
38 DMD with a single-pixel detector for Hadamard-based spectral compressive sensing[55].
39
40
41

42 DMD-based spatially offset Raman spectroscopy

43 Non-invasive chemical depth-profiling of materials is of high interest to a broad range of
44 applications, such as pharmaceutical industry, security, food quality inspection and non-
45 invasive medical diagnosis. Confocal Raman spectroscopy is a popular choice for non-
46 invasive spectral depth-profiling, but the depth range is usually limited to the order of
47 micro-meters. Matousek *et al* [56] introduced a technique called spatially-offset Raman
48 spectroscopy (SORS) that can measure subsurface chemical information from materials
49 eliciting high levels of light scattering. SORS is based on the multiple diffuse scattering of
50 light in turbid media, and involves laterally offset detection relative to the laser excitation
51 spot on the sample.
52
53

54 The implementation of SORS is usually achieved with fiber optics bundles, where optical
55 fibers are arranged in one or more concentric circles to realize spatial offsets for Raman
56
57
58
59
60

1
2
3 photon collection. Since the fibers are fixed in the bundles, these probes lack the ability to
4 change the spatial offsets. Therefore, the range of sample depths is limited by the radii of
5 the concentric circles. Inverse SORS improves the flexibility by delivering the excitation
6 beam with an annular profile at the sample, and detecting the Raman photons through the
7 optical fibers at the center of the probe[57]. Some other methods have also been proposed
8 to achieve adjustable spatial offsets for SORS measurement, but either involves
9 modifications of the mechanical parts in the optical system[58], or have low optical
10 throughput[59].
11
12

13 Liao *et al* recently proposed a novel design to implement SORS by using a DMD added to
14 a conventional Raman spectrometer[60]. The system enables efficient and flexible
15 collection of SORS signals, with software-configurable selection of the spatial offsets,
16 requiring no changes to the optical system or mechanical adjustment. Single-point, annular
17 and multi-offset collection geometries can be easily achieved by altering the pattern
18 displayed on the DMD.
19
20

21 A schematic of the DMD-SORS system is shown in Figure 9(a). The excitation laser is
22 guided into a microscope and focused on to the sample as in a conventional backscattering
23 Raman instrument. Backscattered Raman photons are collected by the objective and
24 focused onto a DMD by a lens. The DMD is placed at a sample-conjugate plane to serve
25 as the spatial offsets controller for SORS measurement, as well as slit/pinhole for the
26 Raman spectrometer.
27
28
29
30
31

32 Figure 9. (a) Schematic of SORS optical system using DMD as a computer-controlled
33 spatially offset mask. (b) single-offset semi-annulus collection geometry with high
34 efficiency. (c) multiple-offset collection geometry with low efficiency. [55] (d) DMD-
35 SORS detection of mineralization through chicken skin and tissue engineering scaffolds
36 [60].
37
38

39 The DMD is at the core of this SORS system, as the spatial offsets are implemented by
40 displaying binary images with annular-like collection patterns. As illustrated in Figure 9(b),
41 a semi-annular pattern consisting of seven collection points is displayed on the DMD. Each
42 point is a group of tiled DMD mirrors ('on' state) that guide the Raman signal toward the
43 spectrometer, while all the black area are mirrors in 'off' state where light is rejected from
44 the spectrometer. These collection points are equally distant from the central point that
45 corresponds to the conjugated point of the laser on the sample, so that an averaged SORS
46 spectrum can be obtained by horizontally shifting and vertically overlapping the stripes of
47 acquired CCD Raman image. The collection points were arranged in a way that there was
48 no more than one point in 'on' state horizontally, so that the crosstalk of Raman spectra on
49 the CCD can be prevented. Vertical gaps of 10 micro-mirrors were retained for the same
50 reason. The actual spatial offset on the sample is determined by the radius of the semi-
51 circle, S , displayed on DMD, and the focal lengths, f_0 and f_m , of the focusing lens in front
52 of the DMD and the microscope objective, respectively. This concentric collection
53 geometry can provide collection efficiency up to $\sim 25\%$, comparable to that of optical fibre
54
55
56
57
58
59
60

1
2
3 bundles with tightly-packed collection fibers. Moreover, the key advantage of DMD-SORS
4 system lies in the fact that the values of spatial offset can be easily changed, as the binary
5 image on DMD is software-configured, and requires no movable mechanical parts. The
6 range of spatial offsets is only restricted by the dimension of active area of the DMD and
7 the CCD sensor. For the initial demonstration, values of spatial offset could be readily
8 selected in the range of 0 – 1 mm using a 2× microscope objective with 90 mm focal length.
9 The capability and flexibility of the DMD-SORS was demonstrated by measuring a two-
10 layer structure consisting of a PMMA sheet as top layer and PS sheet as bottom layer. From
11 Figure 9 (b) we can see, as the value of spatial offset increased from 0 to 1 mm, the Raman
12 band at $\sim 809\text{ cm}^{-1}$ assigned to PMMA decreased gradually, while the intensity of Raman
13 bands assigned to PS increased.
14
15

16
17 To further demonstrate the flexibility of DMD-based SORS, measurements with
18 simultaneous multiple offsets were carried out. A collection geometry using a v-shaped
19 pattern was used, as the points in each arm represent different spatial offsets from the laser
20 excitation position. As depicted in Figure 9 (c), 8 SORS spectra with different offsets can
21 be obtained from the two-layer polymer sample in a single acquisition. Ratiometric data of
22 Raman intensity clearly shows that there was a trend of intensity increase from the bottom
23 layer as the spatial offset increased from 0-1 mm. Since there was only two collection
24 points for each offset, the collection efficiency was reduced compared to concentric semi-
25 circle geometry, led to lower signal to noise ratio of the spectra.
26
27

28
29 Later the authors investigated the feasibility of using DMD-based SORS for non-
30 destructive characterization of bone tissue engineering scaffolds[61]. Raman spectroscopy
31 is a powerful technique for characterization of tissue engineering scaffolds and cells [62,
32 63]. However, measuring molecular signals from the inner parts of the scaffolds is
33 hampered by the high level of optical scattering elicited by these materials. SORS
34 measurements on 3D tissue engineering scaffolds show that hydroxyapatite (HA) can be
35 reliably detected up to depths of 0 – 2.3 mm. Furthermore, SORS detection of HA was also
36 possible when the scaffolds were covered by a 1 mm thick fresh chicken skin (see Figure
37 9(d)). These proof of principle experiments demonstrate the feasibility of using DMD-
38 based SORS for monitoring the in-vitro and in-vivo mineralization of bone tissue
39 engineering scaffolds.
40
41

42 DMD/SPAD-based Time-Gated Raman Spectroscopy

43 Laser-induced fluorescence emission is a major problem in Raman spectroscopy
44 measurements of pigmented samples, including many biological samples. A variety of
45 fluorescent components in tissue give a strong and broad emission that swamp the weak
46 Raman signal. Various strategies have been used to suppress the fluorescence background
47 in the Raman spectra. Laser-induced tissue fluorescence is often spectrally active in the
48 UV and visible range, so it can be effectively avoided in Raman measurement by using an
49 excitation laser with wavelength in the near-infrared (NIR), e.g. 785 nm. However, in
50 many cases, the use of 785-850 nm lasers is still not sufficiently effective when it comes
51 to pigmented biological samples. An excitation wavelength further in the NIR, e.g. 1064
52 nm, can be used to avoid auto-fluorescence, but requires different components for the
53 optical system, in particular InGaAs or Ge CCD detectors. The dark current and read-out
54
55
56
57
58
59
60

1
2
3 noise levels of these detectors are several orders of magnitude higher than the Si CCD used
4 when using lasers with wavelengths shorter than 850 nm. In addition, increasing the
5 wavelength of excitation laser also reduces the efficiency of Raman scattering (Raman
6 efficiency $\sim \lambda^{-4}$). The fact that Raman scattering has a much shorter lifetime (less than a
7 picosecond) than fluorescence emission (range from a few nanoseconds to tens of
8 nanoseconds), makes it possible for separating Raman photons from fluorescence
9 background in the time-domain using time-gating methods.

10
11 Recently, Corden *et al* reported time-gated Raman spectroscopy using a single photon
12 counting detector with a DMD for spectral filtering and multiplexing[64]. The optical
13 system is depicted in Figure 10(a). A pico-second pulsed laser with 60 MHz repetition rate
14 at 775 nm wavelength was employed as excitation source. Similar to previously introduced
15 DMD/PMT-based Raman spectrometer, a combination of a spectrometer and a DMD was
16 used for selecting the photons corresponding to the Raman bands of interest. The
17 collimated Raman scattered and fluorescence photons from the spectrometer were directed
18 onto the DMD, where columns of mirrors were switched 'on' and 'off' to select the desired
19 Raman bands. The selected photons were then fed into a single photon avalanche diode
20 (SPAD) after spectral recombining using two prisms. The SPAD separated the Raman and
21 fluorescence in the time domain, achieving in this way a high level of fluorescence
22 background suppression in the Raman spectra.
23
24
25
26
27
28

29 Figure 10. (a) Schematic of DMD/SPAD-based time-gated Raman spectroscopy system.
30 (b) Bright-field image of the Tylenol and stilbene powder on a glass coverslip (mapping
31 area $120\mu\text{m} \times 120\mu\text{m}$). (c) Time-gated spectra of stilbene (circle) and Tylenol (triangle).
32 The bands used for multiplexing are highlighted. (d) Time-gated Raman spectra at the
33 same locations after the addition of the fluorescing dye on top of the sample. (e) Time-
34 gated Raman maps acquired in the DMD multiplexing mode corresponding to the
35 Tylenol (left) and stilbene (right) bands. Acquisition times: 3 minutes for stilbene maps,
36 27 minutes for the Tylenol maps. (f) Combined pseudo-color Raman map: Tylenol
37 (purple) and stilbene (green); time-gate was 120ps for Tylenol, and 160ps for stilbene,
38 total time: 30 minutes. [64]
39
40

41 To demonstrate the capability of the system for time-gated Raman mapping, a mixture of
42 trans-stilbene and Tylenol powder was covered with a fluorescing dye solution was used
43 (Figure 10(b)). Full Raman spectra of pure trans-stilbene and Tylenol were first acquired
44 by notch DMD scanning, respectively, in order to identify the Raman bands that can be
45 used to discriminate between the two materials, as shown in Figure 10(c-d). Then, the
46 powder mixture with covered by the fluorescing dye solution was imaged by raster
47 scanning. In a first scan shown in Figure 10(e), the columns of DMD mirrors were set to
48 select and multiplex the Raman bands corresponding to trans-stilbene. For the second scan,
49 a different group of mirrors were used for selection of Raman photons from Tylenol.
50 Raman photons were separated from the fluorescence background using a time-gate of 160
51 ps. Figure 10(f) shows the pseudo-color Raman map corresponding to the mixture powder
52 sample, demonstrating that the fluorescence background was effectively suppressed, and
53 the two components in the powder were identified. **While the total imaging time is on a
54 similar time-scale to standard Raman point-mapping (30 minutes for a 40×40 pixels image:**
55
56
57
58
59
60

0.9 s dwell time), the SNR enhancement in the presence of strong fluorescence enables the measurement of previously difficult or even impossible-to-measure samples.

Uses of multiple SLM devices

Multi-focal RMS

Using a high laser power to create multi-foci for excitation of Raman scattering is a promising strategy to improve the acquisition speed of Raman imaging. In principle, the acquisition time can be decreased by a factor equal to the number of laser foci. While various optical elements have been used for generation fixed patterns of multi-foci, such as microlens array[25], diffractive optical elements [65] and galvomirrors [28], Sinjab *et al* developed such a multi-foci Raman micro-spectroscopy system utilizing LC-SLM and DMD[10]. The schematic description of the instrument is shown in Figure 11(a). The LC-SLM generates desired pattern of laser foci, and the DMD in the detection path functions as a software configurable reflective pinhole array. Both the SLM and DMD are synchronized and controlled through software, any changes of the position and number of the laser foci in real time can be rapidly achieved without requiring any hardware alteration.

Figure 11. (a) Schematic description of multi-foci Raman system using SLM and DMD. (b) Simultaneous multi-foci Raman measurements on skin tumor resection for cancer diagnosis.[10]

The authors tested the feasibility of multi-foci RMS for fast cancer diagnosis. RMS has been demonstrated for measuring chemical differences between healthy tissue and tumor with high sensitivity and specificity[66]. However, Raman imaging of large tissue sample is often a long process, makes it unsuitable for intro-operative diagnosis. A multimodal spectral imaging (MSI) combining selective sampling Raman spectroscopy and auto-fluorescence imaging was used to image large tissue samples to detect residual tumour cells[67]. Tissue autofluorescence (AF) imaging were first used to eliminate the non-suspicious area, the remaining part was then used to select and prioritize the sampling points for Raman measurement, with an optimized MSI algorithm allowing high diagnosis accuracy while minimizing the number of Raman acquisition[68]. With this sampling strategy, the time for cancer detection of tissue resections can be effectively shortened, and diagnosis of basal cell carcinoma of surgically resected skin tissue was achieved in 30 minutes[69]. To further increase the speed and diagnosis accuracy, multi-foci RMS was employed for cancer detection after generating sampling points from AF imaging. A CW Ti:Sapphire laser (3 W output, <1 W total at sample) with 785 nm wavelength was used to generate multi-foci created by the LC-SLM, and Raman spectra from six sampling points of skin tissue resections were acquired simultaneously, as shown in Figure 11(b). Diagnosis of large skin tissue samples ($\sim 1 \text{ cm}^2$) obtained in surgery was achieved in 11 minutes, indicating the speed advantage of multi-foci RMS. This initial study demonstrates the potential of this approach to enable intra-operative use of Raman spectroscopy for cancer surgery, in particular for cases where the size of the resected tissue can be as large as several

centimeters, as is in the case of breast cancer [70, 71]. This instrument approach could also be utilized for other selective point-sampling approaches[72, 73].

Multi-focal Raster Scan Imaging

While multi-focal Raman scanning can improve the speed of Raman mapping, cross-talk caused by overlapping laser beams and diffuse scattering of Raman photons reaching the detector can degrade the depth discrimination compared to single-beam confocal Raman microscopy. The SLM/DMD multi-foci Raman system provided the flexibility to investigate the depth-discrimination and speed performance of multi-foci Raman hyperspectral imaging[11]. Multi-focal patterns with different periods were readily realized and used to study the effects of laser foci overlap and Raman signal cross-talk on spectral depth discrimination.

Figure 12. SLM/DMD-based multi-foci confocal Raman imaging. (a) SLM/DMD patterns and corresponding Raman CCD images used for multifocal hyperspectral Raman imaging. (b) Optical sectioning by multi-foci Raman imaging of diphenylalanine micro-tubes.[11]

To investigate the influence of the distance between adjacent laser foci on the depth discrimination of multi-foci confocal Raman system, optical configuration with different distance-to-size ratio (R) were compared. The parameter R refers to the ratio between the distance between the centres of adjacent pinholes D , and the diameter of the pinhole S (Figure 12 (a)). Nine laser foci configuration with R from 2 to 16 were easily achieved without altering any optical components in the system, as the SLM/DMD provided the flexibility to modify the number, location and spacing among the laser foci. Figure 12 (a) shows the Raman CCD images using different laser foci configuration. After optimizing the configuration for fast spectral Raman imaging with good depth discrimination, a 9-beam, $R = 8$ configuration was used for hyperspectral imaging of micro-materials and cells. Figure 12 (b) shows an example of optical sectioning of diphenylalanine micro-tubes, showing good depth discrimination and speed performance highlighting the advantage of SLM/DMD-based multi-foci Raman imaging.

Laser tweezers Raman spectroscopy

Using the LC-SLM/DMD combination in the previous section, but coupled with a much higher NA objective, simultaneous multi-point holographic optical trapping (HOT) and Raman spectroscopy could be carried out[74]. The LC-SLM used was controlled by RedTweezers software developed by Bowman et al.[20], which utilized GPU processing to provide high-speed calculation of phase holograms ($>60\text{Hz}$), allowing real-time and interactive optical manipulation of microparticles. Sinjab et al extended this to incorporate Raman spectroscopy by using the same trapping beams for excitation, and collecting the backscattered Raman light through a dichroic mirror, and imaging the sample plane onto a DMD device to allow the spatial filtering before entering the spectrograph. The performance of the instrument (acquisition times, spatial resolution, spectral resolution etc.) was found to be comparable to single-beam Raman microscopes, which allowed

1
2
3 dynamic Raman micro-spectroscopy measurements to be carried out, as shown in Figure
4 13(a). Here, four polystyrene microparticles were manipulated by the user in software in
5 real-time, whilst Raman spectra were acquired and microscope camera images were
6 acquired (microscope light switched on during first 90s). The read-out was limited to 10Hz
7 (4x10 spectra per second) by the spectrometer shutter.
8
9

10
11
12 Figure 13. Holographic optical trapping Raman micro-spectroscopy. (a) shows video
13 frames and time-course Raman spectra dynamic manipulation-measurement experiment
14 of four trapped 3 μ m polystyrene beads in four regions of the FOV, from which Raman
15 spectra were acquired at 10Hz (total 40 spectra per second). (b) shows multiple trapped
16 cells in different flexible configurations and controlled excitation power to avoid damage.
17 [74]
18

19 Using the HOT-Raman micro-spectroscopy instrument, it was possible to trap and
20 manipulate various cell types, while simultaneously measure their Raman spectra, as
21 shown in Figure 13(b). The sensitivity of particular live cells to persistent laser irradiation
22 was investigated using time-course measurements, by observing changes in the raw data
23 baseline and changes in Raman bands at various laser excitation powers to determine the
24 damage thresholds.
25

26 To demonstrate the unique capability of this approach, the HOT-Raman instrument was
27 used to investigate the spectral changes in human T and dendritic cells during the formation
28 of an immune synapse. Multiple floating T-cells could be optically manipulated into
29 contact with an adherent dendritic cell (DC). After attachment, HOT-Raman spectroscopy
30 was utilized to measure at specific spatial locations of the interacting cell system, to
31 determine differences between junctions and the main cellular bodies. The Raman
32 difference spectra suggested increased protein content at the junction, agreeing with
33 previous studies based on Raman hyperspectral imaging[75].
34
35

36 Future directions & conclusion

37

38
39 We have reviewed the use of SLM devices within the broad field of Raman spectroscopy,
40 highlighting a multitude of novel instrumentation approaches and their various
41 applications. Such devices have many advantages, as they allow real-time software control,
42 increased instrument flexibility, options for automation, and allowing digital signal
43 processing techniques applied to light in spatial, spectral and temporal domains.
44

45
46 LC-SLMs are particularly useful for providing a flexible way of controlling the spatial and
47 temporal properties of the laser excitation in spontaneous and coherent Raman
48 spectroscopies. Examples of this ranged from generating multi-point spontaneous Raman
49 excitation for improved measurement times, to shaping pulsed laser beams to allow
50 coherent Raman spectroscopy using single laser sources.
51

52
53 LC-SLMs have not often been utilized for modulation of Raman scattered photons, likely
54 due to the expected losses in an already Raman weak signal. However, the demonstration
55 of an LC-SLM for compressive sensing by modulating the Raman spectrum shows that
56 high-performance LC-SLMs have sufficient throughput to be useful for applications in
57
58
59

1
2
3 Raman spectroscopy[33]. This feasibility of using an LC-SLM for modulating Raman
4 signals may lead to novel applications in the future.
5

6
7 Other phase modulation devices such as deformable mirrors, which have thus far not been
8 widely utilized in Raman spectroscopy, may offer improvement of aberration
9 correction[14], which has been demonstrated to be useful for focusing within highly
10 scattering tissue for CARS[50]. These devices may also be useful for correcting aberrations
11 in spontaneous Raman hyperspectral imaging on high-background substrates, where it has
12 been shown that spherical aberrations can lead to increase contamination of the Raman
13 spectrum due to the shot noise caused by the Raman photons generated in the substrate
14 even after background subtraction[76].
15

16
17 DMDs have typically been utilized in the detection stages of Raman instruments, as their
18 high reflectivity and fill factor facilitate the necessarily high throughput required for
19 detecting the weak spontaneous Raman scattering signal. Examples included spectral
20 modulation of the Raman signal for computational, compressive, or fluorescence-rejection
21 purposes and sample-conjugate spatial modulation for multi-confocal and spatially-offset
22 Raman measurements.
23

24
25 DMDs could also be utilized for modulation of the Raman excitation laser, for example in
26 Hadamard-encoded imaging, though this would result in significant losses during the
27 patterning process which LC-SLM approaches could reduce. One possibility may include
28 dynamic range enhancement for wide-field Raman excitation, as has been demonstrated
29 for bright-field imaging[77].
30

31
32 Another potential use of DMDs is for periodic shadowing spectroscopy, which is
33 essentially spatial lock-in detection for removal of undesirable stray light. This involves
34 periodic amplitude modulation of light being analysed by a spectrometer along the spatial
35 (slit) axis, with the signal retrieved via a lock-in procedure using the known patterning
36 process as the reference waveform. This was initially demonstrated for a variety of
37 spectroscopy techniques (including CARS) using a fixed Ronchi grating for patterning,
38 and later for emission spectroscopy using a DMD with additional dynamic range
39 enhancement[78, 79]. The latter DMD approach could also be utilized for Raman
40 spectroscopy, and could also be combined with other DMD-based methods as only one
41 spatial axis is required for the shadowing pattern. Spatial patterning can also be used for
42 structured illumination microscopy [80], which has also been demonstrated in Raman
43 micro-spectroscopy using a fixed patterned line illumination[81], which could also use
44 either an LC-SLM or DMD in principle allowing enhanced flexibility in pattern generation.
45
46

47
48 While the focus of this review has been on Raman spectroscopic applications, SLMs may
49 also be of use to infra-red vibrational spectroscopy, particularly due to the limitations of
50 2D detectors in this spectral region. DMDs in particular have been utilized beyond their
51 optical specifications for video-rate single-pixel vibrational imaging of gas leaks at 1500
52 nm [82] and for combined visible/NIR single-pixel microscopy [83]. With the emergence
53 of novel high-power IR sources, it can be expected that many more possibilities will
54 emerge in this direction, particularly as SLM devices operational in the NIR-MIR are
55
56
57
58
59
60

1
2
3 developed further[84]. In addition to SLM optical properties, increased update speeds for
4 pulse-shaping applications would be desirable for some Raman applications where rapid
5 pulse control is required, such as Fourier-transform CARS, which is currently achieved by
6 much faster mechanical scanning processes [85, 86].
7

8
9 In summary, SLM devices have been shown to augment many existing Raman instrument
10 modalities, enhancing several applications in the spatial and spectral domains in the
11 process. In some cases, SLMs have even allowed Raman instrumentation concepts which
12 would otherwise not have been possible at all.
13

14 References

- 15
16
17
18
19
20 [1] S.B. Dierker, C.A. Murray, J.D. Lefrange, N.E. Schlotter. "Characterization of
21 Order in Langmuir-Blodgett Monolayers by Unenhanced Raman Spectroscopy".
22 Chem. Phys. Lett. 1987. 137(5):453–457.
23
24
25
26 [2] C.J. Frank, D.C.B. Redd, T.S. Gansler, R.L. McCreery. "Characterization of Human
27 Breast Biopsy Specimens with Near-IR Raman Spectroscopy". Anal. Chem. 1994.
28 66(3):319–326.
29
30
31
32 [3] B. Yang, M.D. Morris, H. Owen. "Holographic Notch Filter for Low-Wavenumber
33 Stokes and Anti-Stokes Raman Spectroscopy". Appl. Spectrosc. 1991 45(9):1533–
34 1536.
35
36
37
38 [4] M. Delhaye, P. Dhamelincourt. "Raman Microprobe and Microscope with Laser
39 Excitation". J. Raman Spectrosc. 1975. 3(1):33–43.
40
41
42
43 [5] R.M. Stöckle, Y.D. Suh, V. Deckert, R. Zenobi. "Nanoscale Chemical Analysis by
44 Tip-Enhanced Raman Spectroscopy". Chem. Phys. Lett. 2000. 318(1-3):131–136.
45
46
47
48 [6] G.J. Puppels, F.F.M. De Mul, C. Otto, J. Greve, M. Robert-Nicoud, D.J. Arndt-
49 Jovin, T.M. Jovin. "Studying Single Living Cells and Chromosomes by Confocal
50 Raman Microspectroscopy". Nature, 347(6290):301, 1990.
51
52
53
54
55
56
57
58
59
60

- 1
2
3 [7] D.W. Shipp, F. Sinjab, I. Notinger. “Raman Spectroscopy: Techniques and
4 Applications in the Life Sciences”. *Adv. Opt. Photonics*. 2017. 9(2):315–428.
5
6
7
8 [8] L.A. Nafie. “Recent Advances in Linear and Non-Linear Raman Spectroscopy. Part
9 XI”. *J. Raman Spectrosc.* 2017. 48(12):1692–1717.
10
11
12 [9] M. Reicherter, T. Haist, E.U. Wagemann, H.J. Tiziani. “Optical Particle Trapping
13 with Computer-Generated Holograms Written on a Liquid-Crystal Display”. *Opt.*
14 *Lett.* 1999 24(9):608–610.
15
16
17
18 [10] F. Sinjab, K. Kong, G. Gibson, S. Varma, H. Williams, M. Padgett, I. Notinger.
19 “Tissue Diagnosis using Power-Sharing Multifocal Raman Micro-Spectroscopy and
20 Auto-Fluorescence Imaging”. *Biomed. Opt. Express* 2016. 7(8):2993–3006.
21
22
23 [11] Z. Liao, F. Sinjab, H.M. Elsheikha, I. Notinger. “Optical Sectioning in Multifoci
24 Raman Hyperspectral Imaging”. *J. Raman Spectrosc.* 2018. 49(10):1660–1667.
25
26
27 [12] A.M. Weiner. “Femtosecond Pulse Shaping using Spatial Light Modulators”. *Rev.*
28 *Sci. Instrum.* 2000. 71(5):1929–1960.
29
30
31 [13] G.D. Love. “Wave-Front Correction and Production of Zernike Modes with a
32 Liquid-Crystal Spatial Light Modulator”. *Appl. Opt.* 1997. 36(7):1517–1524.
33
34
35 [14] M.J. Booth. “Adaptive Optical Microscopy: the Ongoing Quest for a Perfect Image”.
36 *Light Sci. Appl.* 2014. 3(4):e165.
37
38
39 [15] M.F. Duarte, M.A. Davenport, D. Takhar, J.N. Laska, T. Sun, K.F. Kelly, R.G.
40 Baraniuk. “Single-Pixel Imaging via Compressive Sampling”. *IEEE Signal*
41 *Processing Magazine*. 2008. 25(2):83–91.
42
43
44 [16] V. Studer, J. Bobin, M. Chahid, H.S. Mousavi, E. Candes, M. Dahan. “Compressive
45 Fluorescence Microscopy for Biological and Hyperspectral Imaging”. *Proc. Natl.*
46 *Acad. Sci. U. S. A.* 2012. 109(26):E1679–E1687.
47
48
49
50
51
52
53
54
55
56
57
58
59
60

- 1
2
3 [17] Q.S. Hanley, P.J. Verveer, T.M. Jovin. "Spectral Imaging in a Programmable Array
4 Microscope by Hadamard Transform Fluorescence Spectroscopy". *Appl. Spectrosc.*
5 1999. 53(1):1–10.
6
7
8
9 [18] G.M. Gibson, M. Dienerowitz, P.A. Kelleher, A.R. Harvey, M.J. Padgett. "A Multi-
10 Object Spectral Imaging Instrument". *J. Opt.* 2013. 15(8):085302.
11
12
13 [19] G. Thalhammer, R.W. Bowman, G.D. Love, M.J. Padgett, M. Ritsch-Marte.
14 "Speeding up Liquid Crystal SLMs using Overdrive with Phase Change Reduction".
15 *Opt. Express* 2013. 21(2):1779–1797.
16
17
18 [20] R.W. Bowman, G.M. Gibson, A. Linnenberger, D.B. Phillips, J.A. Grieve, D.M.
19 Carberry, S. Serati, M.J. Miles, M.J. Padgett. "“Red Tweezers”: Fast, Customisable
20 Hologram Generation for Optical Tweezers". *Comput. Phys. Commun.* 2014.
21 185(1):268–273.
22
23
24 [21] R. Bowman, V. D’Ambrosio, E. Rubino, O. Jedrkiewicz, P. Di Trapani, M.J.
25 Padgett. "Optimisation of a Low Cost SLM for Diffraction Efficiency and Ghost
26 Order Suppression". *Eur. Phys. J.: Spec. Top.* 2011. 199(1):149–158.
27
28
29 [22] S. Yabumoto, H.-o. Hamaguchi. "Tilted Two-Dimensional Array Multifocus
30 Confocal Raman Microspectroscopy". *Anal. Chem.* 2017. 89(14):7291–7296.
31
32
33 [23] J. Qi, W.-C. Shih. "Performance of Line-Scan Raman Microscopy for High-
34 Throughput Chemical Imaging of Cell Population". *Appl. Opt.* 2014. 53(13):2881–
35 2885.
36
37
38 [24] D. Wei, S. Chen, Y.H. Ong, C. Perlaki, Q. Liu. "Fast Wide-Field Raman
39 Spectroscopic Imaging Based on Simultaneous Multi-Channel Image Acquisition
40 and Wiener Estimation". *Opt. Lett.* 2016. 41(12):2783–2786.
41
42
43 [25] M. Okuno, H.-o. Hamaguchi. "Multifocus Confocal Raman Microspectroscopy for
44 Fast Multimode Vibrational Imaging of Living Cells". *Opt. Lett.* 2010. 35(24):4096–
45 4098.
46
47
48
49
50
51
52
53
54
55
56
57
58
59
60

- 1
2
3 [26] Y. Kumamoto, Y. Harada, H. Tanaka, T. Takamatsu. "Rapid and Accurate
4 Peripheral Nerve Imaging by Multipoint Raman Spectroscopy". *Sci. Rep.* 2017.
5 7(1):845.
6
7
8
9 [27] L. Kong, P. Zhang, J. Yu, P. Setlow, Y.-q. Li. "Rapid Confocal Raman Imaging
10 using a Synchro Multifoci-Scan Scheme for Dynamic Monitoring of Single Living
11 Cells". *Appl. Phys. Lett.* 2011. 98(21):213703.
12
13
14 [28] L. Kong, M. Navas-Moreno, J.W. Chan. "Fast Confocal Raman Imaging using a 2-D
15 Multifocal Array for Parallel Hyperspectral Detection". *Anal. Chem.* 2015.
16 88(2):1281–1285.
17
18 [29] M. Navas-Moreno, J.W. Chan. "Improving the Imaging Speed of 1064 nm
19 Dispersive Raman Microscopy with Multifocal Patterned Detection". *Opt. Lett.*
20 2017. 42(1):37–40.
21
22 [30] J. Qi, W.-C. Shih. "Parallel Raman Microspectroscopy using Programmable
23 Multipoint Illumination". *Opt. Lett.* 2012. 37(8):1289–1291.
24
25 [31] J. Qi, J. Li, W.-C. Shih. "High-Speed Hyperspectral Raman Imaging for Label-Free
26 Compositional Microanalysis". *Biomed. Opt. Express* 2013. 4(11):2376–2382.
27
28 [32] L. Kong, J. Chan. "A Rapidly Modulated Multifocal Detection Scheme for Parallel
29 Acquisition of Raman Spectra from a 2-D Focal Array". *Anal. Chem.* 2014.
30 86(13):6604–6609.
31
32 [33] B.M. Davis, A.J. Hemphill, D.C. Maltas, M.A. Zipper, P. Wang, D. Ben-Amotz.
33 "Multivariate Hyperspectral Raman Imaging using Compressive Detection". *Anal.*
34 *Chem.* 2011. 83(13):5086–5092.
35
36 [34] D.S. Wilcox, G.T. Buzzard, B.J. Lucier, P. Wang, D. Ben-Amotz. "Photon Level
37 Chemical Classification using Digital Compressive Detection". *Anal. Chim. Acta*
38 2012 755:17–27.
39
40
41
42
43
44
45
46
47
48
49
50
51
52
53
54
55
56
57
58
59
60

- 1
2
3 [35] J.V. Thompson, J.N. Bixler, B.H. Hokr, G.D. Noojin, M.O. Scully, V.V. Yakovlev.
4 “Single-Shot Chemical Detection and Identification With Compressed Hyperspectral
5 Raman Imaging”. *Opt. Lett.* 2017. 42(11):2169–2172.
6
7
8
9 [36] O.G. Rehrauer, V.C. Dinh, B.R. Mankani, G.T. Buzzard, B.J. Lucier, D. Ben-Amotz.
10 “Binary Complementary Filters for Compressive Raman Spectroscopy”. *Appl.*
11 *Spectrosc.* 2018. 72(1):69–78.
12
13
14
15 [37] C. Scotté, H.B. de Aguiar, D. Marguet, E.M. Green, P. Bouzy, S. Vergnole, C.P.
16 Winlove, N. Stone, H. Rigneault. “Assessment of Compressive Raman Versus
17 Hyperspectral Raman for Microcalcification Chemical Imaging”. *Anal. Chem.* 2018.
18 90(12):7197–7203.
19
20
21
22
23 [38] S. Kosmeier, S. Zolotovskaya, A.C. De Luca, A. Riches, C.S. Herrington, K.
24 Dholakia, M. Mazilu. “Nonredundant Raman Imaging using Optical Eigenmodes”.
25 *Optica* 2014. 1(4):257–263.
26
27
28
29 [39] I. Gusachenko, M. Chen, K. Dholakia. “Raman Imaging Through A Single
30 Multimode Fibre”. *Opt. Express* 2017. 25(12):13782–13798.
31
32
33
34 [40] W. Min, C.W. Freudiger, S. Lu, X.S. Xie. “Coherent Nonlinear Optical Imaging:
35 Beyond Fluorescence Microscopy”. *Annu. Rev. Phys. Chem.* 2011. 62:507–530.
36
37
38
39 [41] N. Dudovich, D. Oron, Y. Silberberg. “Single-Pulse Coherently Controlled
40 Nonlinear Raman Spectroscopy and Microscopy”. *Nature* 2002. 418(6897):512.
41
42
43 [42] D. Oron, N. Dudovich, Y. Silberberg. “Single-Pulse Phase-Contrast Nonlinear
44 Raman Spectroscopy”. *Phys. Rev. Lett.* 2002. 89(27):273001.
45
46
47 [43] H. Frostig, O. Katz, A. Natan, Y. Silberberg. “Single-Pulse Stimulated Raman
48 Scattering Spectroscopy”. *Opt. Lett.* 2011. 36(7):1248–1250.
49
50
51
52 [44] B. von Vacano, T. Backup, M. Motzkus. “Highly Sensitive Single-Beam Heterodyne
53 Coherent Anti-Stokes Raman Scattering”. *Opt. Lett.* 2006. 31(16):2495–2497.
54
55
56
57
58
59
60

- 1
2
3 [45] J. Rehbinder, L. Brückner, A. Wipfler, T. Buckup, M. Motzkus. “Multimodal
4 Nonlinear Optical Microscopy with Shaped 10 fs Pulses”. *Opt. Express* 2014.
5 22(23):28790–28797.
6
7
8
9 [46] H. Frostig, T. Bayer, N. Dudovich, Y.C. Eldar, Y. Silberberg. “Single-Beam
10 Spectrally Controlled Two-Dimensional Raman Spectroscopy”. *Nat. Photonics* 2015.
11 9(5):339.
12
13
14
15 [47] C.W. Freudiger, W. Min, G.R. Holtom, B. Xu, M. Dantus, X.S. Xie. “Highly
16 Specific Label-Free Molecular Imaging with Spectrally Tailored Excitation-
17 Stimulated Raman Scattering (STE-SRS) Microscopy”. *Nat. Photonics* 2011.
18 5(2):103.
19
20
21
22
23 [48] H. Tu, Y. Liu, D. Turchinovich, M. Marjanovic, J.K. Lyngsø, J. Lægsgaard, E.J.
24 Chaney, Y. Zhao, S. You, W.L. Wilson, B. Xu, M. Dantus S.A. Boppart. “Stain-Free
25 Histopathology by Programmable Supercontinuum Pulses”. *Nat. Photonics* 2016.
26 10(8):534.
27
28
29
30
31 [49] M.R. Beversluis, S.J. Stranick. “Enhanced Contrast Coherent Anti-Stokes Raman
32 Scattering Microscopy using Annular Phase Masks”. *Appl. Phys. Lett.* 2008.
33 93(23):231115.
34
35
36
37 [50] A.J. Wright, S.P. Poland, J.M. Girkin, C.W. Freudiger, C.L. Evans, X.S. Xie.
38 “Adaptive Optics for Enhanced Signal in CARS Microscopy”. *Opt. Express* 2007.
39 15(26):18209–18219.
40
41
42
43 [51] E. Da Silva, N.Q. Dao, M.D. Jouan. “New Raman Spectrometer Using a Digital
44 Micromirror Device and a Photomultiplier Tube Detector for Rapid On-Line
45 Industrial Analysis. Part I: Description of the Prototype and Preliminary Results”.
46 *Appl. Spectrosc.* 2008. 62(3):279–284.
47
48
49
50
51
52
53
54
55
56
57
58
59
60

- 1
2
3 [52] E.P. Wagner, B.W. Smith, S. Madden, J.D. Winefordner, M. Mignardi.
4 "Construction and Evaluation of a Visible Spectrometer using Digital Micromirror
5 Spatial Light Modulation". *Appl. Spectrosc.* 1995. 49(11):1715–1719.
6
7
8
9 [53] D. Cebeci, B. Mankani, D. Ben-Amotz. "Recent Trends in Compressive Raman
10 Spectroscopy Using DMD-Based Binary Detection". *J. Imaging* 2019. 5(1):1.
11
12
13 [54] D.S. Wilcox, G.T. Buzzard, B.J. Lucier, O.G. Rehrauer, P. Wang, D. Ben-Amotz.
14 "Digital Compressive Chemical Quantitation and Hyperspectral Imaging". *Analyst*
15 2013. 138(17):4982–4990.
16
17
18 [55] P. Berto, C. Scotté, F. Galland, H. Rigneault, H.B. De Aguiar. "Programmable
19 Single-Pixel-Based Broadband Stimulated Raman Scattering". *Opt. Lett.* 2017.
20 42(9):1696–1699.
21
22
23 [56] P. Matousek, I.P. Clark, E.R.C. Draper, M.D. Morris, A.E. Goodship, N. Everall,
24 M. Towrie, W.F. Finney, A.W. Parker. "Subsurface Probing in Diffusely Scattering
25 Media using Spatially Offset Raman Spectroscopy". *Appl. Spectrosc.* 2005.
26 59(4):393–400.
27
28
29 [57] P. Matousek. "Inverse Spatially Offset Raman Spectroscopy for Deep Noninvasive
30 Probing of Turbid Media". *Appl. Spectrosc.* 2006. 60(11):1341–1347.
31
32
33 [58] K.M. Khan, S.K. Majumder, P.K. Gupta. "Cone-Shell Raman Spectroscopy (CSRS)
34 for Depth-Sensitive Measurements in Layered Tissue". *J. Biophotonics* 2015. 8(11-
35 12):889–896.
36
37
38 [59] Z. Wang, H. Ding, G. Lu, X. Bi. "Use of a Mechanical Iris-Based Fiber Optic Probe
39 for Spatially Offset Raman Spectroscopy". *Opt. Lett.* 2014. 39(13):3790–3793.
40
41
42 [60] Z. Liao, F. Sinjab, G. Gibson, M. Padgett, I. Notingher. "DMD-Based Software-
43 Configurable Spatially-Offset Raman Spectroscopy for Spectral Depth-Profiling of
44 Optically Turbid Samples". *Opt. Express* 2016. 24(12):12701–12712.
45
46
47
48
49
50
51
52
53
54
55
56
57
58
59
60

- 1
2
3 [61] Z. Liao, F. Sinjab, A. Nommets-Nomm, J. Jones, L. Ruiz-Cantu, J. Yang, F. Rose,
4 I. Notingher. “Feasibility of Spatially Offset Raman Spectroscopy for In Vitro and In
5 Vivo Monitoring Mineralization of Bone Tissue Engineering Scaffolds”. *Anal.*
6 *Chem.* 2016. 89(1):847–853.
7
8
9
10
11 [62] I. Notingher, A.R. Boccaccini, J. Jones, V. Maquet, L.L. Hench. “Application of
12 Raman Microspectroscopy to the Characterisation of Bioactive Materials”. *Mater.*
13 *Charact.* 2002. 49(3):255–260.
14
15
16
17 [63] S. Powell T.S. Leung. “Highly Parallel Monte-Carlo Simulations of the Acousto-
18 Optic Effect in Heterogeneous Turbid Media”. *J. Biomed. Opt.* 2012. 17(4):045002.
19
20
21 [64] C.J. Corden, D.W. Shipp, P. Matousek, I. Notingher. “Fast Raman Spectral Mapping
22 of Highly Fluorescing Samples by Time-Gated Spectral Multiplexed Detection”.
23 *Opt. Lett.* 2018. 43(23):5733–5736.
24
25
26
27 [65] A.Z. Samuel, S. Yabumoto, K. Kawamura, K. Iwata. “Rapid Microstructure
28 Characterization of Polymer Thin Films with 2D-Array Multifocus Raman
29 Microspectroscopy”. *Analyst* 2015. 140(6):1847–1851.
30
31
32
33 [66] K. Kong, C. Kendall, N. Stone, I. Notingher. “Raman Spectroscopy for Medical
34 Diagnostics—From In-Vitro Biofluid Assays to In-Vivo Cancer Detection”. *Adv.*
35 *Drug Delivery Rev.* 2015. 89:121–134.
36
37
38
39 [67] K. Kong, C.J. Rowlands, S. Varma, W. Perkins, I.H. Leach, A.A. Koloydenko, H.C.
40 Williams, I. Notingher. “Diagnosis of Tumors During Tissue-Conserving Surgery
41 with Integrated Autofluorescence and Raman Scattering Microscopy”. *Proc. Natl.*
42 *Acad. Sci. U. S. A.* 2013. 201311289.
43
44
45
46 [68] S. Takamori, K. Kong, S. Varma, I. Leach, H.C. Williams, I. Notingher.
47 “Optimization of Multimodal Spectral Imaging for Assessment of Resection Margins
48 During Mohs Micrographic Surgery for Basal Cell Carcinoma”. *Biomed. Opt.*
49 *Express* 2015. 6(1):98–111.
50
51
52
53
54
55
56
57
58
59
60

- 1
2
3 [69] R. Boitor, K. Kong, D. Shipp, S. Varma, A. Koloydenko, K. Kulkarni, S. Elsheikh,
4 T.B. Schut, P. Caspers, G. Puppels, I. Notingher. “Automated Multimodal Spectral
5 Histopathology for Quantitative Diagnosis of Residual Tumour During Basal Cell
6 Carcinoma Surgery”. *Biomed. Opt. Express* 2017. 8(12):5749–5766.
7
8
9
10
11 [70] K. Kong, F. Zaabar, E. Rakha, I. Ellis, A. Koloydenko, I. Notingher. “Towards Intra-
12 Operative Diagnosis of Tumours During Breast Conserving Surgery by Selective-
13 Sampling Raman Micro-Spectroscopy”. *Phys. Med. Biol.* 2014. 59(20):6141.
14
15
16
17 [71] D.W. Shipp, E.A. Rakha, A.A. Koloydenko, R.D. Macmillan, I.O. Ellis, I.
18 Notingher. “Intra-Operative Spectroscopic Assessment of Surgical Margins During
19 Breast Conserving Surgery”. *Breast Cancer Res.* 2018. 20(1):69.
20
21
22
23 [72] C.J. Rowlands, S. Varma, W. Perkins, I. Leach, H. Williams, I. Notingher. “Rapid
24 Acquisition of Raman Spectral Maps Through Minimal Sampling: Applications in
25 Tissue Imaging”. *J. Biophotonics* 2012. 5(3):220–229.
26
27
28
29 [73] K. Kong, C.J. Rowlands, H. Elsheikha, I. Notingher. “Label-Free Molecular
30 Analysis of Live *Neospora Caninum* Tachyzoites in Host Cells by Selective
31 Scanning Raman Micro-Spectroscopy”. *Analyst* 2012. 137(18):4119–4122.
32
33
34
35 [74] F. Sinjab, D. Awuah, G. Gibson, M. Padgett, A.M. Ghaemmaghami, I. Notingher.
36 “Holographic Optical Trapping Raman Micro-Spectroscopy for Non-Invasive
37 Measurement and Manipulation of Live Cells”. *Opt. Express* 2018. 26(19):25211–
38 25225.
39
40
41
42
43 [75] A.B. Zoladek, R.K. Johal, S. Garcia-Nieto, F. Pascut, K.M. Shakesheff, A.M.
44 Ghaemmaghami, I. Notingher. “Label-Free Molecular Imaging of Immunological
45 Synapses Between Dendritic and T Cells by Raman Micro-Spectroscopy”. *Analyst*
46 2010. 135(12):3205–3212.
47
48
49
50
51
52
53
54
55
56
57
58
59
60

- 1
2
3 [76] F. Sinjab, G. Sicilia, D.W. Shipp, M. Marlow, I. Notinger. "Label-Free Raman
4 Hyperspectral Imaging of Single Cells Cultured on Polymer Substrates". *Appl.*
5 *Spectrosc.* 2017. 71(12):2595–2607.
6
7
8
9 [77] A.A. Adeyemi, N. Barakat, T.E. Darcie. "Applications of Digital Micro-Mirror
10 Devices to Digital Optical Microscope Dynamic Range Enhancement". *Opt. Express*
11 2009. 17(3):1831–1843.
12
13
14 [78] E. Kristensson, J. Bood, M. Alden, E. Nordström, J. Zhu, S. Huldt, P.-E. Bengtsson,
15 H. Nilsson, E. Berrocal, A. Ehn. "Stray Light Suppression in Spectroscopy Using
16 Periodic Shadowing". *Opt. Express* 2014. 22(7):7711–7721.
17
18
19 [79] E. Kristensson, A. Ehn, E. Berrocal. "High Dynamic Spectroscopy Using a Digital
20 Micromirror Device and Periodic Shadowing". *Opt. Express* 2017. 25(1):212–222.
21
22
23 [80] M.G.L. Gustafsson. "Surpassing the Lateral Resolution Limit by a Factor of Two
24 Using Structured Illumination Microscopy". *J. Microsc.* 2000. 198(2):82–87.
25
26
27 [81] K. Watanabe, A.F. Palonpon, N.I. Smith, A. Kasai, H. Hashimoto, S. Kawata, K.
28 Fujita. "Structured Line Illumination Raman Microscopy". *Nat. Commun.* 2015.
29 6:10095.
30
31
32 [82] G.M. Gibson, B. Sun, M.P. Edgar, D.B. Phillips, N. Hempler, G.T. Maker, G.P.A.
33 Malcolm, M.J. Padgett. "Real-Time Imaging of Methane Gas Leaks Using A Single-
34 Pixel Camera". *Opt. Express* 2017. 25(4):2998–3005.
35
36
37 [83] N. Radwell, K.J. Mitchell, G.M. Gibson, M.P. Edgar, R. Bowman, M.J. Padgett.
38 "Single-Pixel Infrared and Visible Microscope". *Optica* 2015. 1(5):285–289.
39
40
41 [84] K. Fan, J.Y. Suen, W.J. Padilla. "Graphene Metamaterial Spatial Light Modulator for
42 Infrared Single Pixel Imaging". *Opt. Express* 2017. 25(21):25318–25325.
43
44
45 [85] K. Hashimoto, M. Takahashi, T. Ideguchi, K. Goda. "Broadband Coherent Raman
46 Spectroscopy Running at 24,000 Spectra Per Second". *Sci. Rep.* 2016. 6:21036.
47
48
49
50
51
52
53
54
55
56
57
58
59
60

- 1
2
3 [86] M. Tamamitsu, Y. Sakaki, T. Nakamura, G.K. Podagatlapalli, T. Ideguchi, K. Goda.
4
5 “Ultrafast Broadband Fourier-Transform CARS Spectroscopy at 50,000 Spectra/s
6
7 Enabled by a Scanning Fourier-Domain Delay Line”. *Vib. Spectrosc.* 2017. 91:163–
8
9 169.
10
11
12
13
14
15
16
17
18
19
20
21
22
23
24
25
26
27
28
29
30
31
32
33
34
35
36
37
38
39
40
41
42
43
44
45
46
47
48
49
50
51
52
53
54
55
56
57
58
59
60

For Peer Review